Boundary Layer Separation on Isolated Boattail Nozzles

By

William Kelly Abeyounis

B. S. May 1973, North Carolina State University

A Thesis submitted to

The Faculty of

The School of Engineering and Applied Science

of The George Washington University in partial satisfaction

of the requirements for the degree of Master of Science

May 8, 1977

Thesis directed by

Dr. Richard W. Barnwell

Associate Professorial Lecturer in Engineering

ABSTRACT

An investigation has been conducted in the Langley 16-foot transonic tunnel at free-stream Mach numbers from 0.40 to 0.95 at 0° angle of attack to study the phenomenon of separated flow on a series of circular-arc afterbodies. Both high-pressure air and solid circular cylinders with a diameter equal to the nozzle exit diameter were used to simulate jet exhausts. A detailed data base of boundary layer separation locations was obtained using oil-flow techniques.

The results of this investigation indicate that boundary layer separation is most extensive on steep boattails at high Mach numbers. Changes in the jet total-pressure ratio (jet total to free-stream static) affect the extent of separation very little; however, entrainment associated with the presence of a jet has a significant effect when compared to solid simulator data. Several separation criteria were evaluated using experimental data. No criterion in general accurately predicted the separation locations for the solid simulator cases. The best results were obtained by curve-fitting a modified Reshotko-Tucker criterion with experimental data.

ACKNOWLEDGEMENTS

I would like to thank all of those who gave me assistance in the preparation of this paper. I am indebted to the National Aeronautics and Space Administration for giving me the opportunity to pursue graduate study and for providing the time and facilities necessary for this investigation.

I would especially like to acknowledge the contributions of Dr. Richard W. Barnwell, my advisor, whose advice was greatly appreciated. I would like to thank Ms. Dorothy P. Wright and Ms. Debbie L. Griffith for typing this paper. Also, I would like to thank Ms. Kathryn H. Peddrew and Ms. Margaret L. Hurt for their help in preparing the figures. In addition, I would like to thank Mr. L. E. Putnam for his advice and his adaptation of the boundary-layer computer program used herein.

TABLE OF CONTENTS

LIST OF SYMBOLS

A	cross-sectional area, m^2
a	intercept of linear least-squares curve
b	slope of linear least-squares curve
C	constant in Stratford criterion
C_f	local skin friction coefficient, $\frac{\tau_w}{q_\ell}$
C_p	pressure coefficient based on free-stream conditions, $\frac{p_\ell - p_\infty}{q_\infty}$
$\hat{C}_p$	pressure coefficient based on conditions at the minimum static pressure on the boattail, $\frac{p'_\ell - p_o}{q_o}$
$\bar{C}_p$	modified pressure coefficient in Stratford criterion, $1 - \left(\frac{M_\ell}{M_o}\right)^2$
d	diameter, m
E	standard error of estimate, $\sqrt{\frac{\sum_1^n [y_i - (a + bz_i)]^2}{n-2}}$
F	ratio of boundary-layer thickness at the minimum static pressure to that at separation defined in equation 4 in Presz criterion, $\frac{\delta_o}{\delta_{sep}}$
G	ratio of boundary-layer thickness at the minimum static pressure to that at separation defined in equation 5 in Presz criterion, $\frac{\delta_o}{\delta_{sep}}$

$\dot{I}$	momentum of entrained mass flow in Presz criterion, N
l	length of boattail, m
$\dot{m}$	entrained mass flow in Presz criterion, $\frac{kg}{sec}$
N_{Re}	Reynolds number, $\frac{u_\infty d_m}{\nu_\infty}$
n	number of points in linear least-squares curve
p	pressure, N/m^2
q	dynamic pressure, N/m^2
R	boattail circular-arc radius, m
r	radial distance from center line of model, m
S	nozzle convergence length, m
s	axial coordinate in nozzle convergence section, m
$\hat{s}$	streamwise distance along body, m
$\bar{s}$	effective streamwise distance along body in Stratford criterion, m
T	temperature, K
t	nozzle throat length, m
u	velocity component in $\hat{s}$ direction, m/sec
X	axial distance aft from model nose, m
x	axial distance aft from start of boattail, m
v	dependent variable in linear least-squares curve
z	independent variable in linear least-squares curve
β	terminal boattail angle, deg
β_c	boattail chord angle, deg
γ	specific heat ratio
Δx	axial distance from the minimum static pressure on the boattail to boundary layer separation, $x_{sep} - x_o$, m

δ	boundary-layer thickness, m
δ^*	boundary-layer displacement thickness, m
θ	boundary-layer momentum thickness, m
ν	kinematic viscosity, m^2/sec
ρ	density, kg/m^3
τ_w	wall shear stress, N/m^2

Subscripts

b	base
DP	dewpoint
e	exit
fs	ficticious stagnation point
j	jet
ℓ	local
m	maximum
o	boattail minimum static pressure point
p	predicted
ps	preseparation
s	plume simulator
sep	separation point
t	stagnation
1	boundary layer edge, top edge of control volume in Presz criterion
∞	free-stream

LIST OF FIGURES

CHAPTER I

INTRODUCTION

The nacelle afterbody is a critical area as far as aircraft performance is concerned. The flow in this region can be extremely complex, and therefore hard to predict. The external flow goes through an expansion and then a compression (ref. 1); it also interacts with the jet plume. This phenomenon causes the afterbody boundary layer to thicken, and in many cases separate. In cases in which boundary layer separation does occur, the pressure distribution and drag on the afterbody greatly differ from those of unseparated cases (ref. 1). This fact has led to much experimental work in the area (refs. 1 to 9); however, little detailed separation data is available from which improved analytical techniques can be developed.

Presently there are many theoretical methods for predicting afterbody flows (refs. 9 to 33). Most of these employ a potential flow calculation coupled with a boundary layer calculation. Some of the boundary-layer methods are designed to predict and calculate separated flows implicitly. Others approach the problem by predicting the separation location using simpler, semiempirical techniques (refs. 34 to 52) and modeling the separated region as a solid cone frustum (ref. 37). Good results have been obtained for cases with unseparated boattail flows (ref. 1). For separated flow cases, however, the difficulty in correctly modeling the complex flow near afterbodies has caused the theoretical results obtained up to now to be inaccurate.

In order to better understand boattail flow separation and to determine what criteria can best predict it for use in patched inviscid/viscid solutions, an oil-flow study was conducted in the Langley 16-foot transonic tunnel using a series of circular-arc afterbodies (ref. 1). The investigation was conducted at free-stream Mach numbers from 0.40 to 0.94 at 0° angle of attack. Air was used to simulate jet exhausts with jet total-pressure ratios (jet total to free-stream static) varying from jet-off up to about 9, depending upon the configuration and the free-stream Mach number. Solid cylinders were also used to simulate the jets at the on-design condition. (The flow conditions for which pressure data was available in references 1 to 3 were repeated as closely as possible during the oil-flow tests.) The primary goal of the test was to establish a systematic data base from which the dependency of flow separation on such factors as the free-stream Mach number, the longitudinal surface curvature, and the jet total-pressure ratio could be determined. (Since a single model was used for the test, and the tunnel is an atmospheric tunnel, it was possible only to test over a limited Reynolds number range. For this reason, the effect of Reynolds number was not included in the data base.) The experimental results will be reported in this paper. An evaluation of several of the semiempirical techniques for predicting flow separation will also be presented.

CHAPTER II

EXPERIMENTAL APPARATUS AND PROCEDURE

Wind Tunnel Description

This flow separation study was conducted in the Langley 16-foot transonic tunnel. The tunnel is a single-return, continuous, atmospheric tunnel. Its test section has octagonal cross sections with slots at each of the eight corners. The free-stream Mach number is continuously variable from 0.20 to 1.30. A more detailed description of the Langley 16-foot tunnel can be found in references 53 to 55.

Model and Support System Description

The model used in this investigation was an isolated, single-engine nacelle model, to which various circular-arc boattail nozzles could be attached. A sketch of a typical configuration, in which high-pressure air was used to simulate the jet exhaust, is shown in figure 1. The nacelle model had a rounded shoulder at the junction of the conical nose and the cylindrical section. The nozzles were attached at station 111.76 cm. Nozzle boattails for all configurations started at station 121.92 cm. The dry, high-pressure air used for jet simulation had a stagnation temperature of about 274 K. It was piped through a sting-strut, which supported the model, into the high-pressure plenum. The air then flowed radially outward (perpendicular to the model axis) into the low-pressure plenum through eight multi-holed sonic nozzles. The nozzles were equally spaced around the circumference of the high-pressure plenum. The flow then accelerated

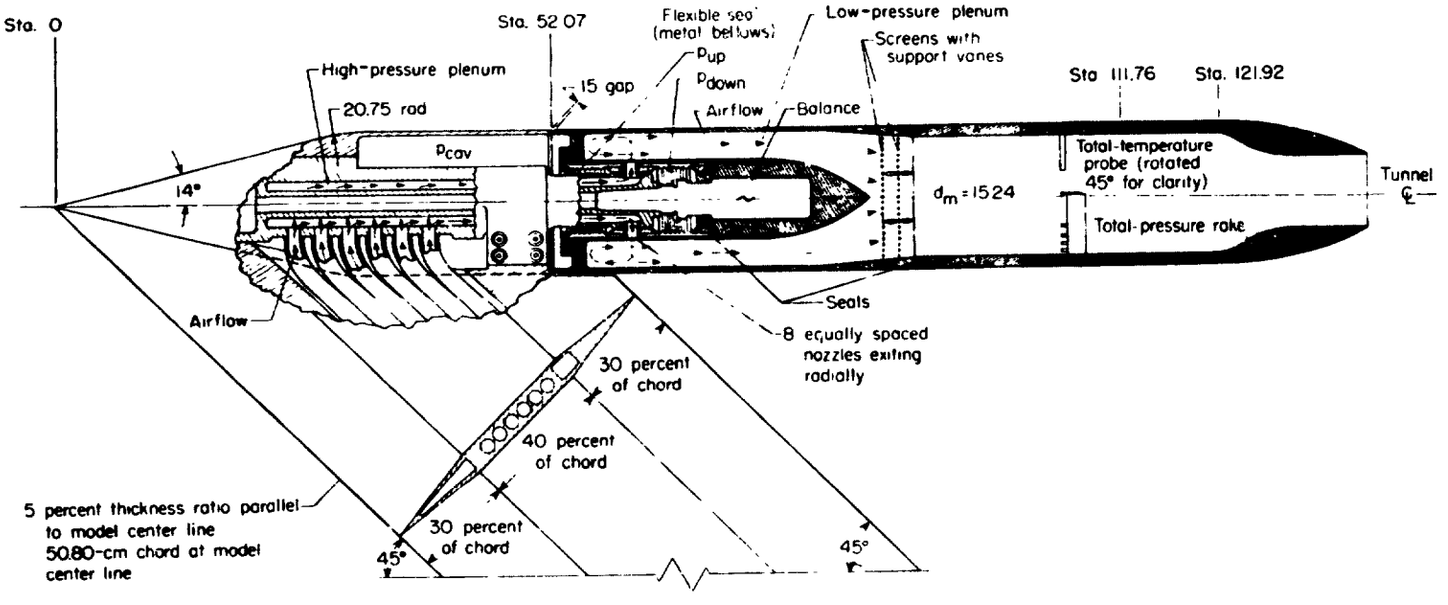

Figure 1.- Sketch of air-powered cone-cylinder model with a typical circular-arc convergent nozzle installed. All dimensions are in centimeters unless otherwise noted.

rearward, passing through flow-smoothing screens in the model tailpipe. These screens, supported by four vanes, consisted of a 0.635-cm mesh formed using 0.0635-cm wire. Figure 2 is a photograph of the air-powered model installed in the Langley 16-foot transonic tunnel.

Solid cylinders were also used to simulate jet exhausts. Figure 3 illustrates a configuration typical of those tested. An internal sting was installed in the single-engine nacelle model to support the solid simulators. Figure 4 shows one of these configurations installed in the Langley 16-foot transonic tunnel. Only simulators with a diameter equal to the nozzle exit diameter ($d_s/d_e = 1.0$) were tested. All simulators were 27.94 cm long. It was felt this was long enough so that base effects of the simulator would be negligible on the boattails.

The model was mounted in the tunnel on a sting-strut support system. As shown in figures 1 to 5, the nose of the model was attached to the strut blade. The blade was swept 45° and was 5 percent thick with a 50.8-cm chord. The sting was 5.08 cm by 10.16 cm in cross section, with the top and bottom capped with half-cylinders of 2.54-cm radius. The center line of the sting was located 55.88 cm below the wind-tunnel center line. This placed the axis of the model on the tunnel center line and the nose of the model at tunnel station 39.93 meters. Cross-sectional area distributions of the model and support system are shown in figure 5. The model blockage was 0.099 percent of the cross-sectional area of the test section; the maximum blockage of the model and support system was 0.148 percent.

Figure 2.- Air-powered model with configuration 8 attached, installed in the Langley 16-foot transonic tunnel.

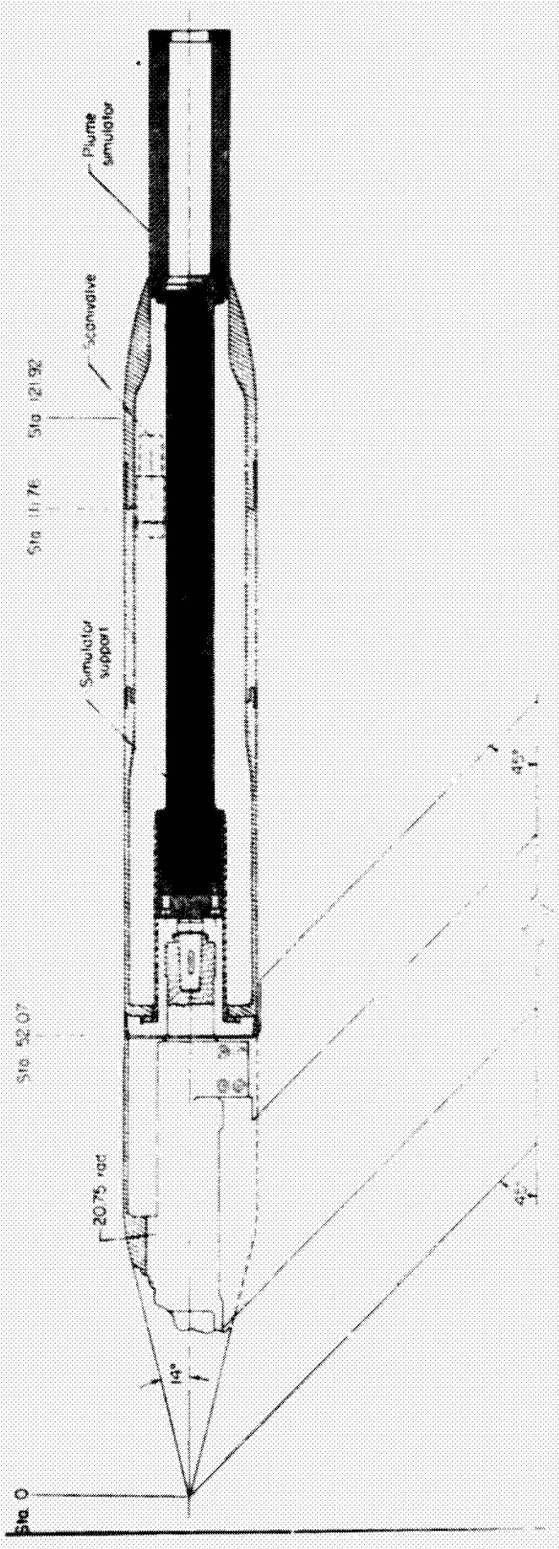

Figure 3.- Sketch of cone-cylinder nacelle model showing internal sting arrangement for support of simulators.

Figure 4.- Nacelle model installed in the Langley 16-foot transonic tunnel with typical circular-arc afterbody and $d_s/d_e = 1.00$ simulator attached.

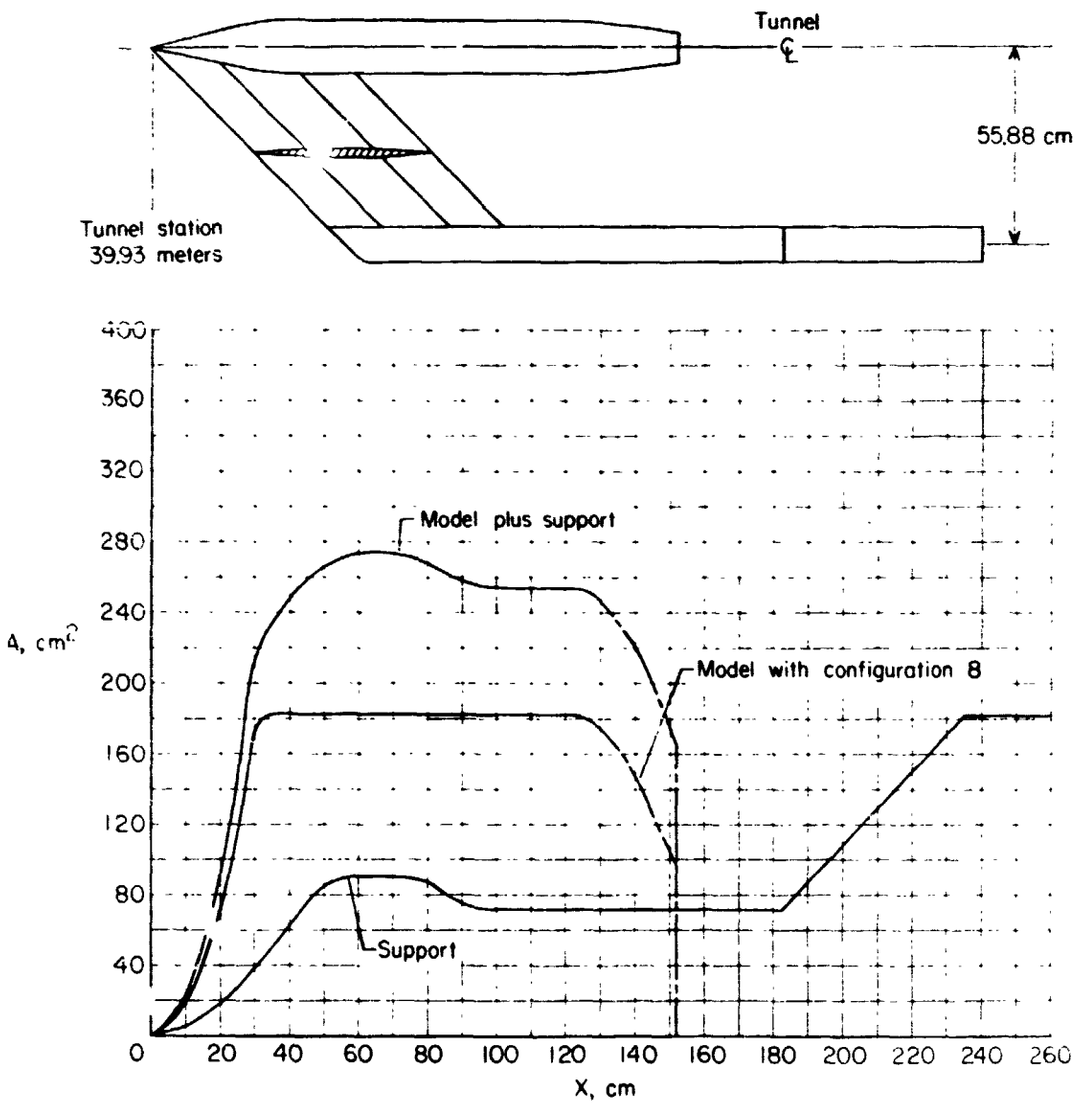

Figure 5.- Sketch of model and support system with corresponding cross-sectional area distributions.

Afterbody Model Description

A family of eight circular-arc afterbodies was available for testing. Figure 6 shows sketches and corresponding tables of dimensions for these nozzle afterbodies. The internal contour of each nozzle was basically an ASME long-throat nozzle (ref. 56). Some modifications were necessary because the external contours set limits within which the internal contours had to contract from a fixed internal diameter to the required exit diameter. Also, space had to be allotted for tube routing. All of the nozzles had throats with circular cross sections.

Instrumentation and Test Procedure

The eight afterbody models and their solid simulators were equipped with static-pressure orifices. The orifice locations and static-pressure data used in this paper were presented in reference 1. For the cases in which air was used to simulate jet exhausts, jet total-pressure measurements were obtained by using an internally-mounted total-pressure rake (fig. 6). The jet total pressures were measured using electrical strain gage pressure transducers calibrated to an accuracy of ± 0.5 percent of the gage capacity (6.89×10^5 N/m^2).

All testing was conducted in the Langley 16-foot transonic tunnel at free-stream Mach numbers ranging from 0.40 to 0.94 and at an angle of attack of 0°. The model attitude was not changed during the test. The tunnel upflow (on the order of 0.1 degree throughout the free-stream Mach number range) and sting deflection (known to be extremely small) were not taken into account. Boundary layer transition was fixed

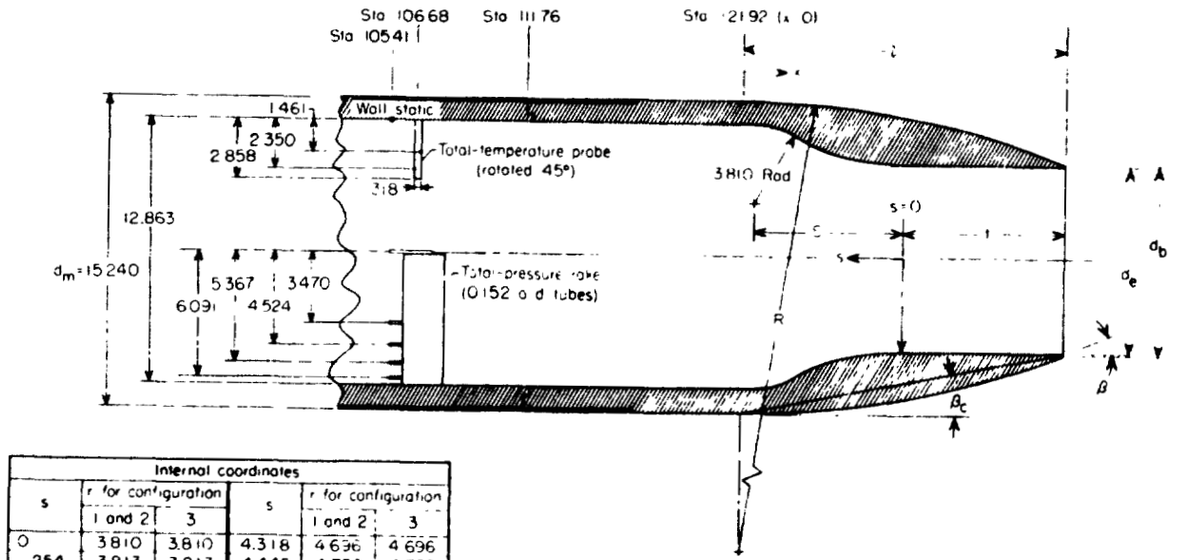

Internal coordinates					
s	r for configuration		s	r for configuration	
	1 and 2	3		1 and 2	3
0	3810	3810	4318	4696	4696
254	3813	3813	4445	4755	4755
508	3820	3820	4572	4816	4816
762	3835	3835	4699	4882	4882
1016	3856	3856	4826	4948	4948
1270	3881	3881	4953	5019	5019
1524	3912	3912	5080	5090	5090
1778	3950	3950	5207	5169	5169
2032	3993	3993	5334	5248	5248
2286	4041	4041	5461	5334	5334
2540	4097	4097	5588	5420	5420
2794	4161	4161	5715	5514	5514
3048	4229	4229	5842	5611	5611
3302	4308	4308	5969	5715	5715
3556	4392	4392	6096	5822	5822
3810	4483	4483	6223	5939	——
3937	4534	4534	6350	6060	——
4064	4585	4585	6477	6190	——
4191	4641	4641			

Geometric parameters								
Configuration	ℓ/d_m	d_e/d_m	d_b/d_m	R/d_m	l/d_m	S/d_m	β, deg	β_c, deg
1	0800	050	051	1429	0.50	0533	34054	17027
2	1.000	50	51	2163	.50	533	27533	13.766
3	1768	50	51	6500	50	458	15781	7891

(a) Configurations 1 to 3.

Figure 6.- Detailed sketch of typical configuration with tables of geometric parameters and internal coordinates. All dimensions are in centimeters unless otherwise noted.

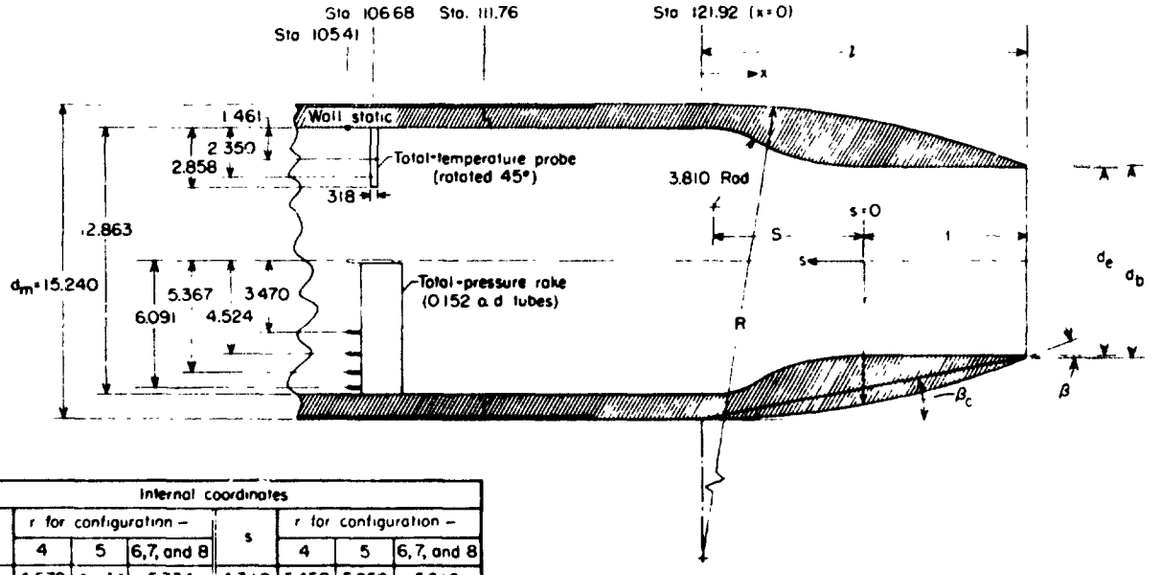

Internal coordinates							
s	r for configuration –			s	r for configuration –		
	4	5	6, 7, and 8		4	5	6, 7, and 8
0	4.572	[illegible]	5.334	4.318	5.458	5.052	5.618
.254	4.575	[illegible]	5.337	4.445	5.517	—	—
.508	4.582	[illegible]	5.339	4.572	5.578	5.123	5.659
.762	4.597	[illegible]	5.342	4.699	5.644	—	—
1.016	4.618	[illegible]	5.349	4.826	5.710	5.202	5.705
1.270	4.643	[illegible]	5.357	4.953	5.781	5.245	—
1.524	4.674	[illegible]	5.364	5.080	5.852	5.291	[illegible]
1.778	4.712	[illegible]	5.377	5.207	5.931	5.339	[illegible]
2.032	4.755	[illegible]	5.390	5.334	6.010	5.392	[illegible]
2.286	4.803	[illegible]	5.405	5.461	6.096	5.448	[illegible]
2.540	4.859	[illegible]	5.423	5.588	6.182	5.512	[illegible]
2.794	4.923	[illegible]	5.443	5.715	6.276	5.578	[illegible]
3.048	4.991	[illegible]	5.466	5.842	6.373	5.654	[illegible]
3.302	5.070	[illegible]	5.489	5.969	6.477	5.738	[illegible]
3.556	5.154	[illegible]	5.517	6.096	6.584	5.839	[illegible]
3.810	5.245	[illegible]	5.547	6.223	6.701	5.961	[illegible]
3.937	5.296	—	—	6.350	6.822	6.137	[illegible]
4.064	5.347	4.991	5.580	6.431	—	6.431	[illegible]
4.191	5.403	—	—				

Geometric parameters								
Configuration	l/d_m	d_e/d_m	d_b/d_m	R/d_m	l/d_m	S/d_m	β, deg	β_c, deg
4	1.00	.060	.061	2.662	0.500	0.462	22.068	11.034
5	1.50	.60	.61	5.867	.592	.536	14.814	7.407
6	1.00	.70	.71	3.521	.367	.507	16.507	8.250
7	1.50	.70	.71	7.831	.667	.507	11.043	5.521
8	2.00	.70	.71	13.866	.833	.507	8.293	4.147

(b) Configurations 4 to 8.

Figure 6.- Concluded.

by a 0.254-cm strip of No. 100 grit located 2.54 cm from the tip of the nose, using the techniques described in references 57 and 58.

High-pressure air was used to simulate jet exhausts with jet total-pressure ratios varying from jet-off up to 9, depending upon the configuration and free-stream conditions. Solid cylinders were also used to simulate the on-design condition. This jet total pressure range covers that typically used in subsonic flight by transports and fighters.

Since the Langley 16-foot transonic tunnel is an atmospheric tunnel, the tunnel free-stream conditions vary with the ambient conditions. The range of free-stream conditions is shown as a function of the free-stream Mach number in figure 7. The oil-flow study consisted of several runs. In each run, a particular configuration was tested. Each run consisted of a sweep of free-stream Mach numbers. For configurations which used high-pressure air to simulate jet exhausts, a sweep of nozzle total-pressure ratios was conducted at each Mach number. In an effort to minimize the tunnel total temperature variation, data was generally taken at the highest Mach number first, and then at progressively lower Mach numbers. At each data point (i.e. each Mach number and/or nozzle total-pressure ratio setting at which data was recorded), tunnel conditions were allowed to stabilize, at which time 10 frames of data were taken over a 10 second period. The 16-foot tunnel has a small cyclic variation in the flow with a period of about 10 seconds. The average of the 10 frames of data was therefore used for each point to minimize errors in the measured quantities resulting from this cylic variation.

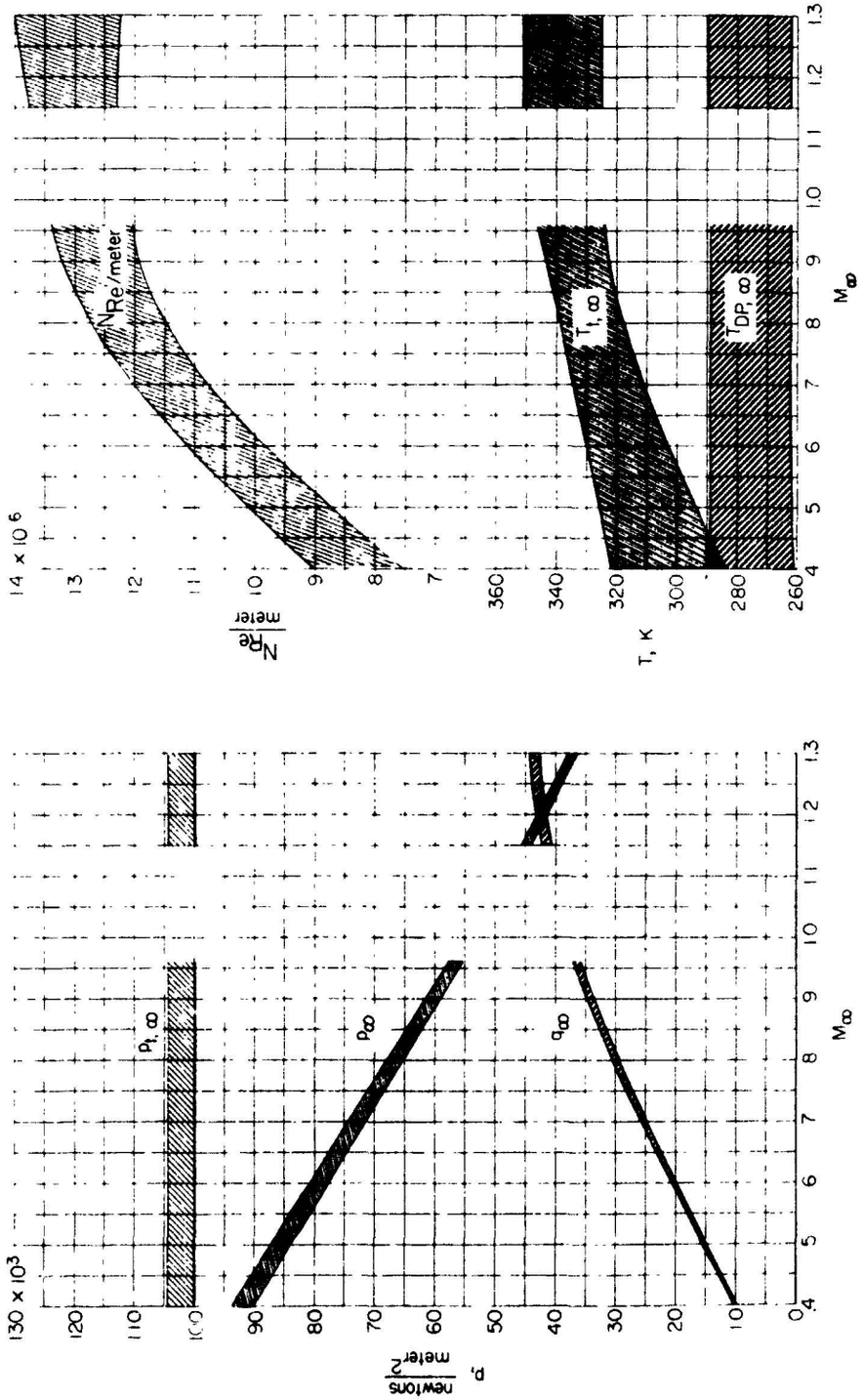

Figure 7.- Band of the free-stream parameters encountered during the investigation.

To obtain oil-flow data, the aft portion of the model was painted with 100-weight oil before each run, and repainted as often as was necessary to insure good oil-flow quality. Photographs were taken using a camera mounted on the top flat of the test section. In order to make the oil fluoresce, the photographs were taken under ultraviolet light. To check for hysterecis, some conditions were repeated during a run, going up and coming down in Mach number.

Data Reduction

Separation locations were obtained from the oil-flow photographs. A photograph of a grid held next to the model before a run was used to scale distances. Separation distances were measured at the top of the boattail because of the possibility of support-strut interference. References 2 and 3 and some unpublished data indicate that the top can be assumed to be interference free. Photographs were also checked to see if there was too much oil on the model.

CHAPTER III

RESULTS AND DISCUSSION

Experimental Results

Typical photographs obtained during this oil-flow investigation are presented as figures 8, 9, and 10. They illustrate some of the problems encountered while making oil-flow tests. One problem is getting the proper amount of oil on the model. There must be enough oil of a high enough viscosity to remain on the model the length of time needed for the tunnel to reach the test conditions. Conversely, the oil must have a low enough viscosity to react to changes in flow conditions within a reasonable length of time, and be present in a layer thin enough to not greatly alter the effective body shape. Another problem is measuring the separation locations since the separation line is usually not straight. Generally the line is curved, conforming to a series of vortices spaced around the body in the separated region. This phenomenon, similar to Taylor and Goertler vortices (ref. 59), is characteristic of turbulent flow, and perhaps is triggered by small asymmetries in the flow. Figure 8 also shows a line in the separated region near the nozzle exit. This indicates that a two-cell vortex pattern may exist in the separated region, at least at high jet total-pressure ratios.

Some factors influencing the location of the separation point are the free-stream Mach number, the longitudinal curvature of the model, and the jet plume entrainment and blockage. The Reynolds number also affects the separation location; however, it was not possible to test

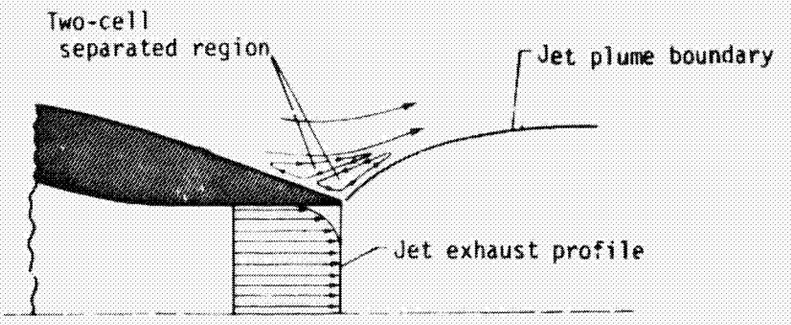

(a) Two-cell vortex model.

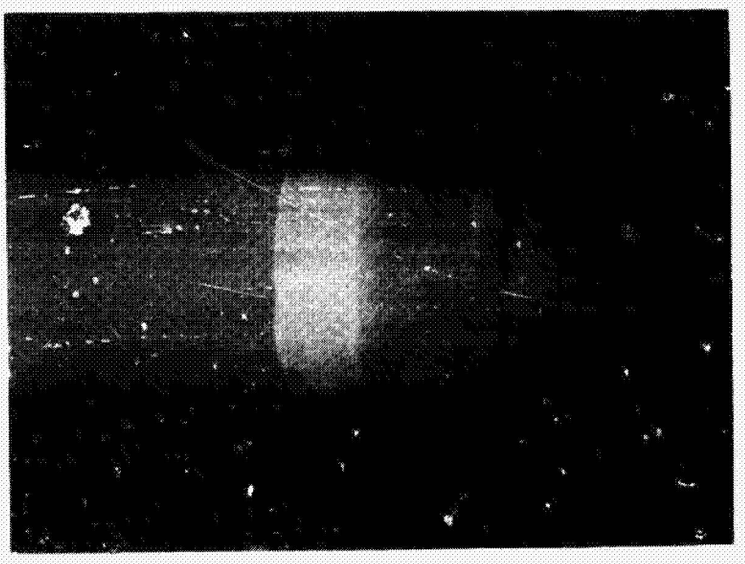

(b) $\ell/d_m = 1.0$, $d_e/d_m = 0.50$, $M_\infty = 0.90$, $p_{t,j}/p_\infty = 7.83$

Figure 8. - Example of two-cell vortex separation.

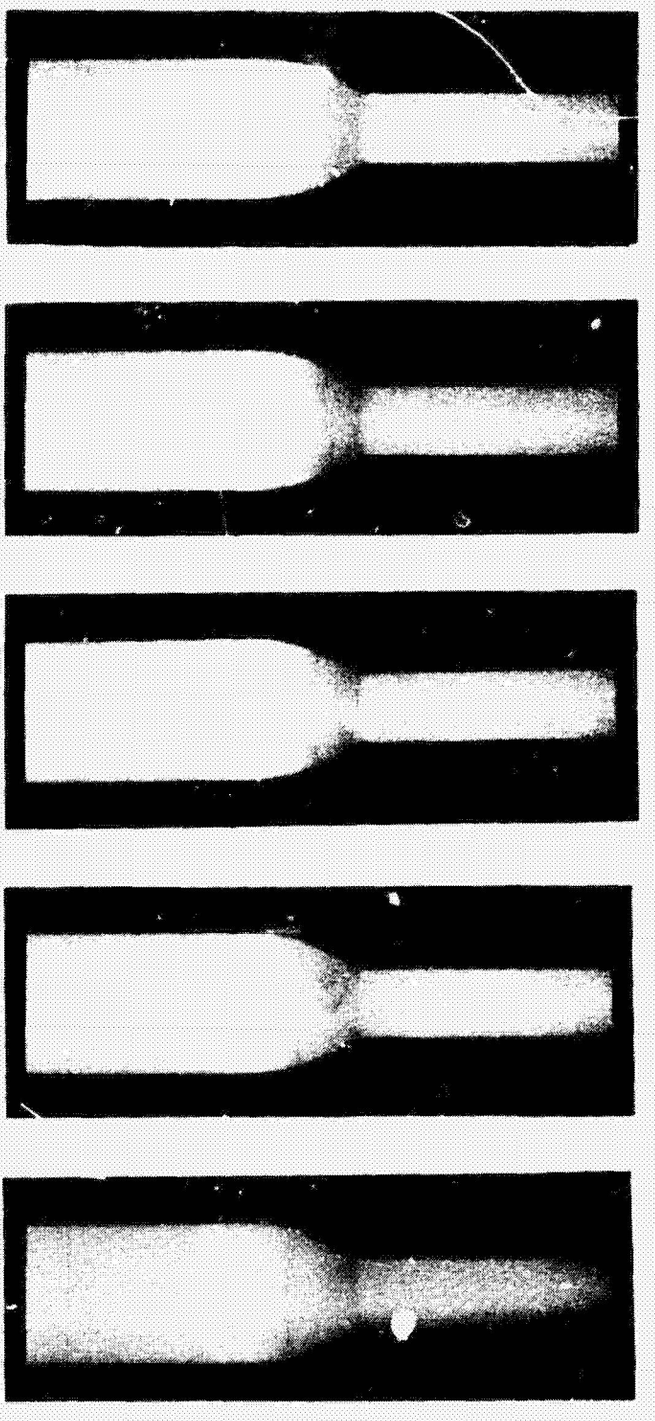

Figure 9. - Oil-flow photographs showing the effect of Mach number on separation location.

(ι/d_m = 0.80, d_e/d_m = 0.50)

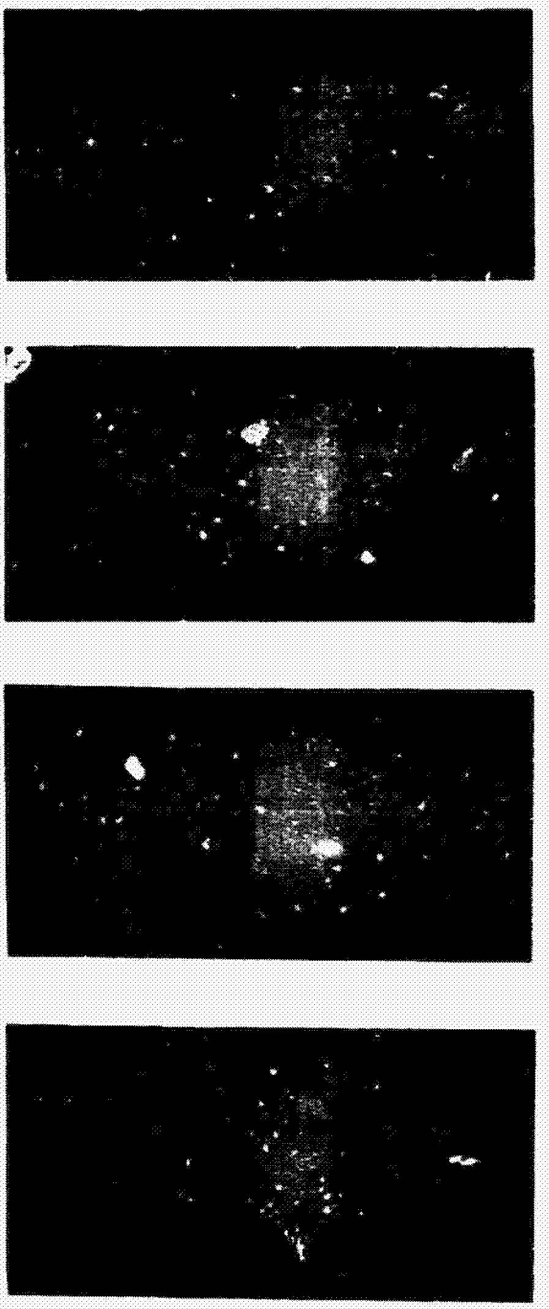

$P_{t,j}/P_\infty = 4.04$

Figure 10.- Oil-flow photographs showing the effect of jet total-pressure ratio on separation location.
($M_\infty = 0.9$, $l/d_j = 1$ 0.50)

over a wide Reynolds number range since the tunnel is an atmospheric tunnel and only one model was used in the test. For subsonic flow, the separation point moved forward on a given configuration as the free-stream Mach number increased. (See figures 9 and 11.) For transonic flows (free-stream Mach numbers above about 0.8, depending upon the configuration), pressure distributions indicate that a shock probably existed on the boattail when the flow decelerated from supersonic to subsonic speeds (ref. 1). When this happened, the boundary layer separation probably became shock induced. The separation point moved forward on the boattail to a point in the vicinity of the shock. It is speculated that the shock-induced separated region combined with the previously described separated region to cause this movement. This may explain the large shifts in the separation location at transonic speeds which occurred for two of the configurations.

The longitudinal curvature of the boattail also greatly affected the separation location. As expected, for a given free-stream Mach number, the most forward separation location occurred on the steepest boattail configuration. As the longitudinal curvature progressively decreased from configuration to configuration, the separation location moved rearward. Only on the four steepest boattail configurations was any separation ever found over the free-stream Mach number range tested.

The entrainment and blockage of the jet plume are functions of the jet total-pressure ratio. It is seen in figures 10 and 12 that the separation location changed little over the jet total-pressure

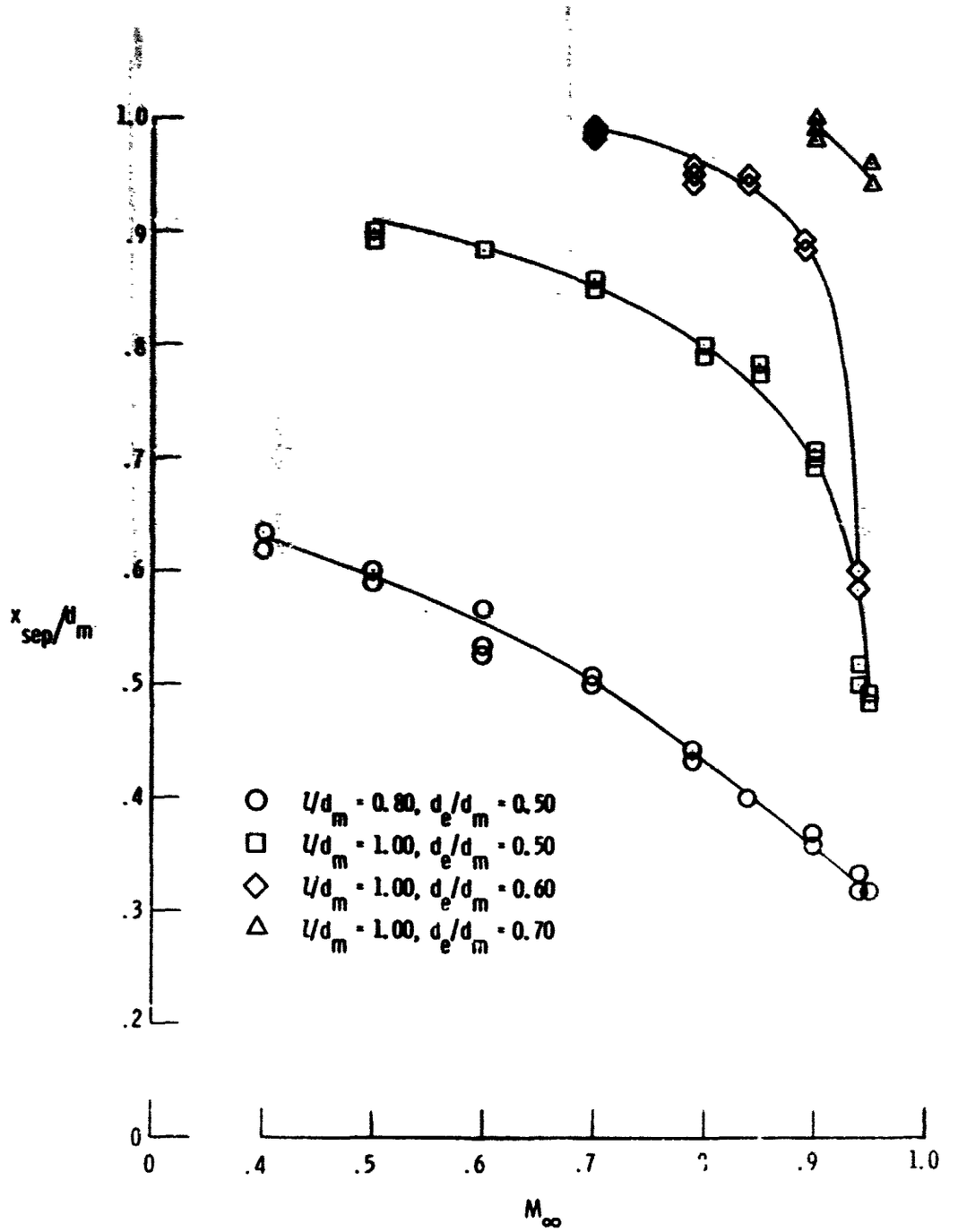

Figure 11.- Separation locations for configurations using a solid cylinder to simulate jet exhausts.

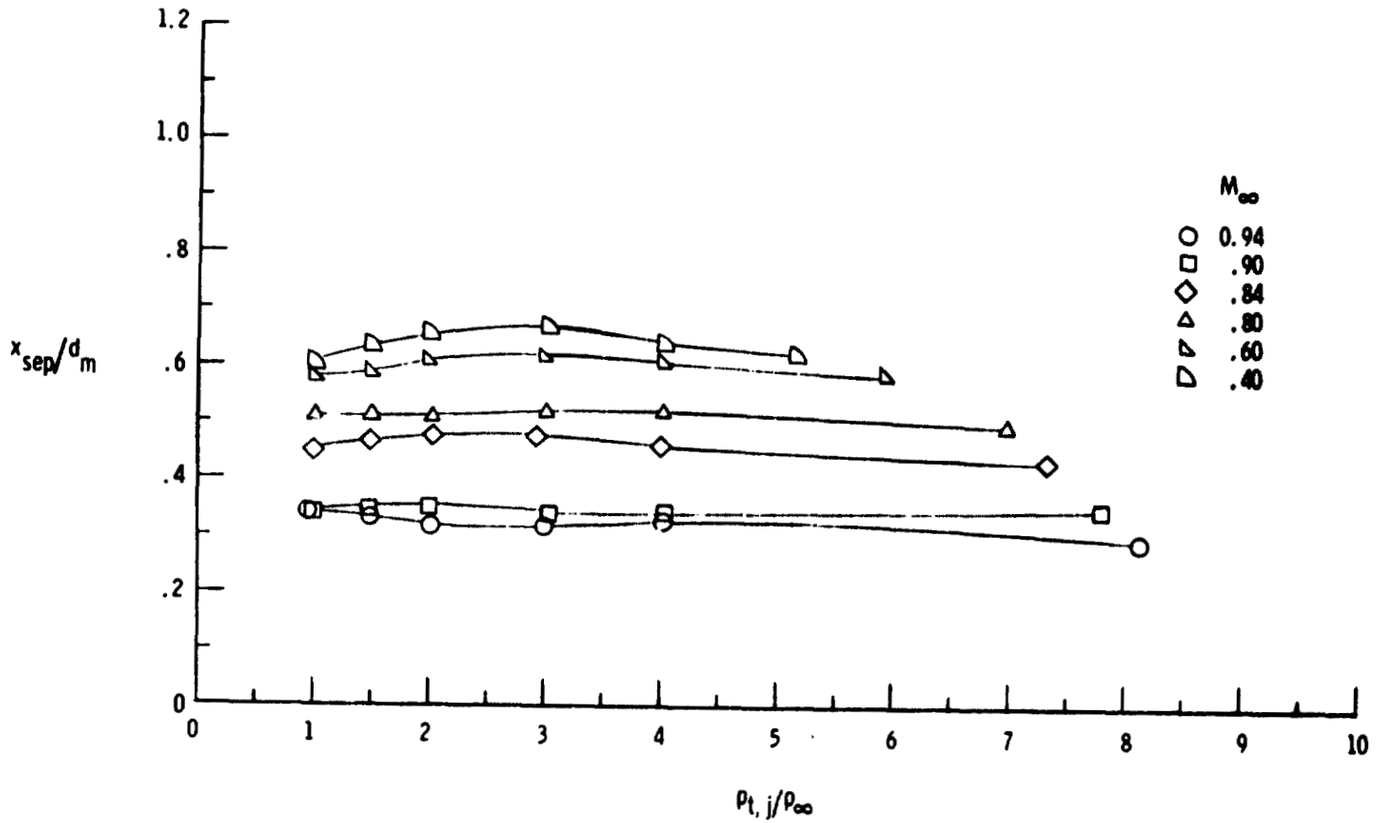

(a) Configuration 1 (ℓ/d_m = 0.80, d_e/d_m = 0.50)

Figure 12.- Separation locations for configurations using high-pressure air to simulate jet exhausts.

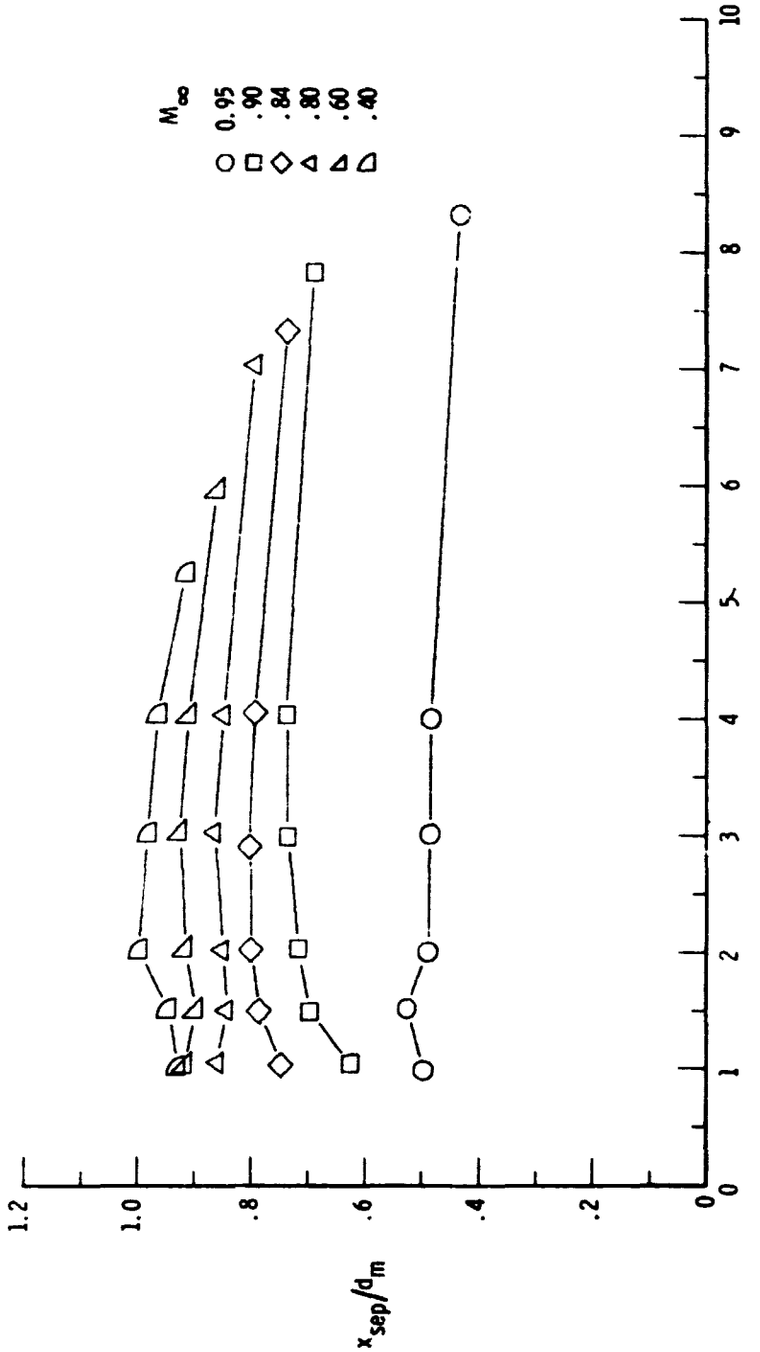

(b) Configuration 2 (l/d_m = 1.0, d_e/d_m = 0.50);

Figure 12. - Continued.

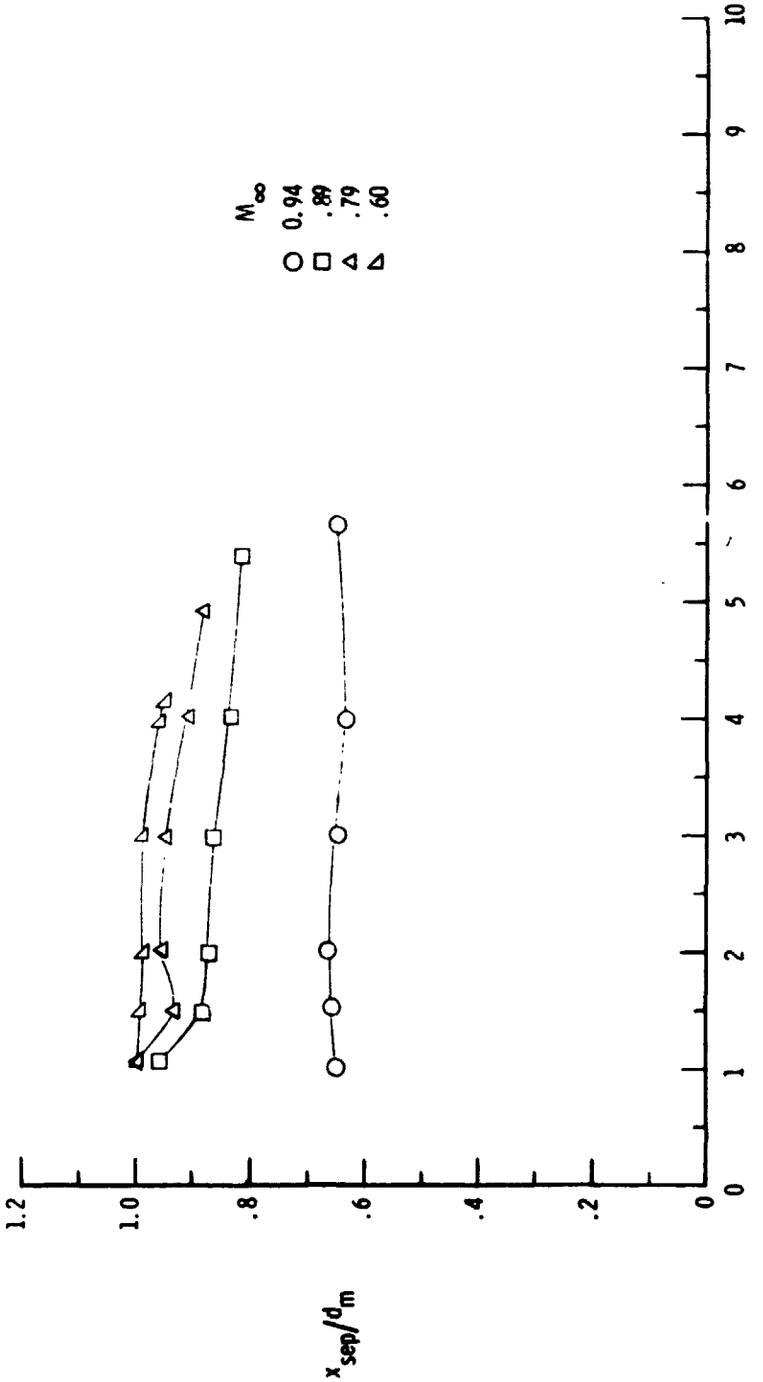

(c) Configuration 4 (l/d_m = 1.0, d_e/d_m = 0.60)

Figure 12. - Continued.

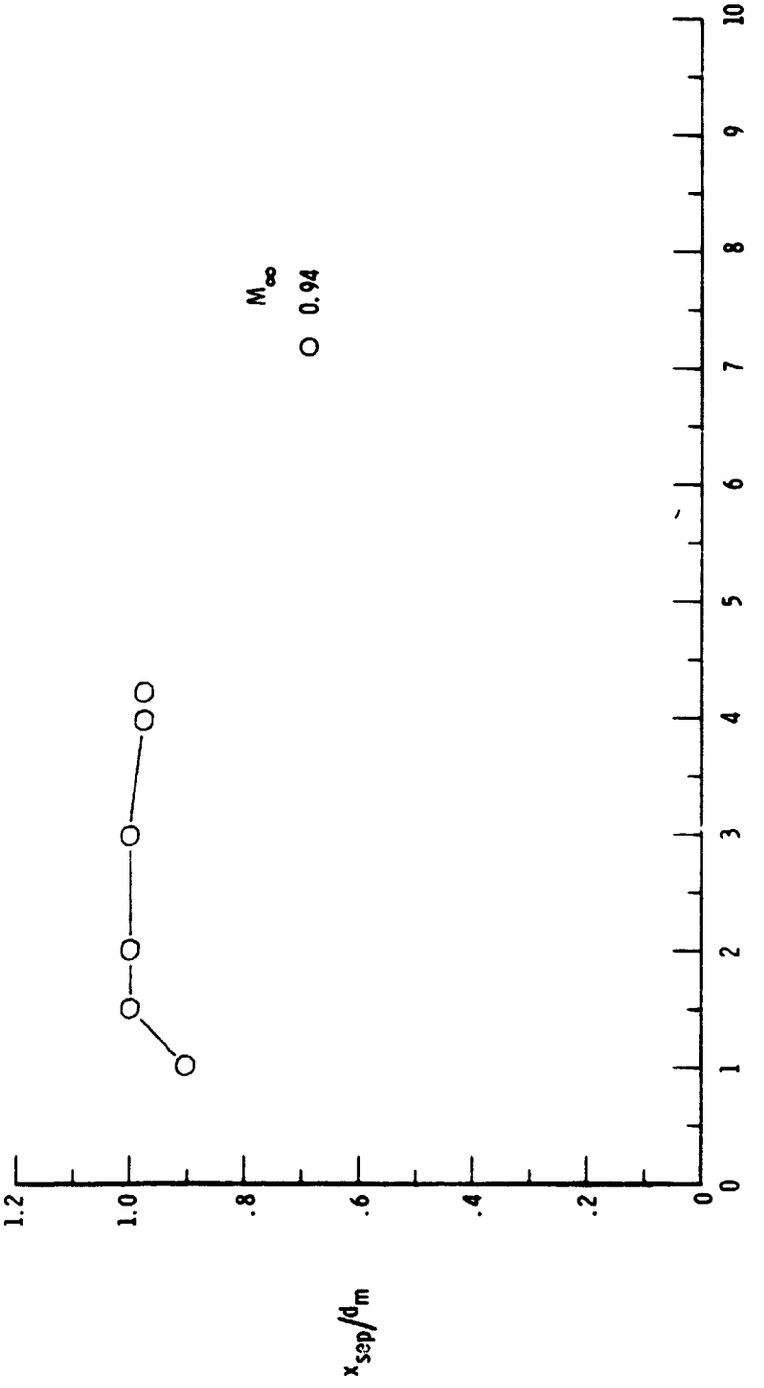

(d) Configuration 6 (ℓ/d_m = 1.0, d_e/d_m = 0.70)

Figure 12. - Concluded.

ratio range tested. (The level of some of the data curves may be in error because of an excess of oil on the model. The data in question are at the free-stream Mach number of 0.84 for configuration 1, 0.85 and 0.40 for configuration 2, and 0.94 for configurations 4 and 6.) The flatness of the curves probably indicates that the changes in entrainment and blockage effects induced by varying the jet total-pressure ratio were nearly equal in magnitude and opposite in effect.

The jet entrainment tends to move the separation location rearward on the boattail by entraining mass from the separated region rearward into the jet. The magnitude of entrainment is a function of both the velocity difference and "surface" area between flows. Therefore, for a convergent nozzle with a given free-stream condition, the mass entrained into the jet would tend to increase as the jet-exit velocity increased. This increase in jet-exit velocity corresponds to an increase in the nozzle total-pressure ratio. If the jet velocity is less than the external velocity, the external flow actually tends to entrain mass from the jet. Also, some mixing occurs since the external flow contacts the jet flow at an angle and must be turned by the jet flow. When the on-design condition is reached, the jet-exit Mach number equals one, and remains constant for higher jet total-pressure ratios. Consequently, the jet-exit velocity also remains constant. The velocity in the jet plume increases with higher jet total-pressure ratios; however, since the jet-exit velocity is constant, the velocity increases near the boattail are relatively small. Consequently, the entrainment tends to level off.

While entrainment tends to move the separation location

rearward, blockage effects of jets tend to pressurize the boattail and move the separation location forward. As the jet total-pressure ratio is increased up to the on-design condition, the separation location moves rearward. As higher total-pressure ratios are reached, the plume blockage effects increase, halting the rearward movement of the separation location and eventually causing a slight forward movement. There appears to be a disparity in some of the jet-off ($p_{t,j}/p_\infty = 1.0$) data. Aside from experimental error, this may be due in part to unsteadiness which can occur in base flow cases. (Reference 60 presents a theoretical approach to the base flow problem.) Also, at the higher Mach numbers, the separation location is more sensitive to small errors in setting the Mach number in the wind tunnel.

Since the separation location remains almost stationary throughout the jet total-pressure ratio range, it seems likely that solid simulator data could be used to estimate the jet-on separation locations. However, figure 13 shows that a difference exists in the separation locations obtained for on-design conditions between the solid simulator data and the high-pressure air data. The jet total-pressure ratio at which the on-design condition occurs varies slightly for differing Mach numbers and configurations, causing some of the difference. However, since the separation location changes little throughout the range of jet total-pressure ratios, most of the difference between solid simulator and high-pressure air separation data must be due to entrainment. For subsonic cases,

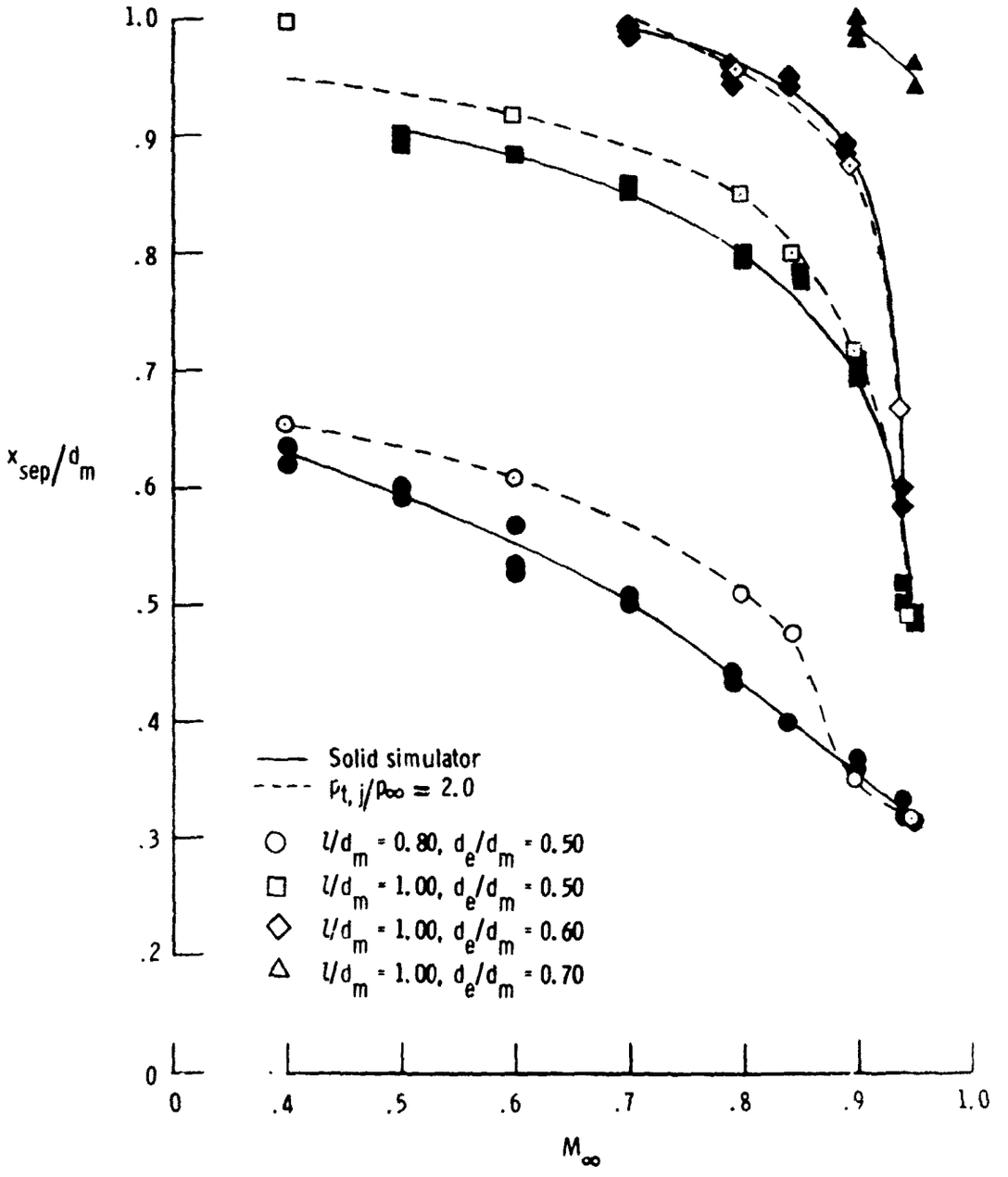

Figure 13.- Comparison of separation locations obtained through the use of solid simulators with those obtained from jet operation at $p_{t,j}/p_\infty = 2$.

this difference in separation locations obtained using the two jet simulation techniques appears to be mainly a function of the "surface" area of the separated region washed by the jet (the region between the jet exit and the reattachment point on the plume). This tends to directly correspond to the extent of separation on the boattail. For transonic cases, shock-induced separation probably occurs. Within experimental accuracy, the difference in the data curves reduces to almost zero. This indicates that the shock location is probably not greatly affected by entrainment.

Theoretical Results

Using this newly acquired data base, several flow separation criteria were evaluated. Most of these criteria were simple, semi-empirical methods. A patched inviscid/viscid interaction computer program consisting of a potential flow calculation (ref. 11) and a momentum-integral boundary layer calculation (ref. 12) was used to compute the needed boundary layer and inviscid flow parameters. The criteria were applied using both the experimental and theoretical inviscid pressure distributions as input to the boundary-layer program. There were several advantages in using the inviscid pressure distributions. The inviscid pressure distributions do not contain the scatter inherent in experimental data, and they are easily calculated. This experimental scatter (especially in the minimum pressure) can cause large deviations in the separation predictions of some criteria. Also a criterion based on the inviscid pressure distribution could provide a simpler, noninteractive, and cheaper

solution. By contrast, a criterion based on experimental data might be more useful in an interactive scheme to solve a flow field.

One of the criteria tested was a modified form of the Reshotko-Tucker criterion (ref. 49):

$$\frac{M_{sep}}{M_o} = 0.762 \qquad (1)$$

which states that the ratio of the Mach number at separation to the Mach number at the minimum pressure point is a constant. This criterion is derived by applying the momentum and moment of momentum integral equations with special functions of the boundary layer shape factor. The shear stress terms are assumed negligible in comparison to pressure terms. This criterion was modified during the present investigation to better fit experimental data by incorporating the effect of Reynolds number through the skin friction coefficient at the minimum pressure point $C_{f,o}$ to yield:

$$\frac{M_{sep}}{M_o \sqrt[5]{C_{f,o}}} = 2.622 \qquad (2)$$

This modified form will hereafter be referred to simply as the Reshotko-Tucker criterion.

Another criterion evaluated was the Page criterion (ref. 34):

$$\hat{C}_{p,sep} = \frac{p_{\ell,sep} - p_o}{q_o} = 0.38 \qquad (3)$$

This simple criterion states that separation occurs where the pressure coefficient based on the minimum static pressure reaches 0.38.

A third method is the Presz criterion (ref. 37). The separation location is determined by using the following equations:

$$F = \frac{p_{sep} M_{sep} \sqrt{2 + (\gamma - 1)M_{sep}^2} (1 - \delta^*/\delta)_{sep}}{(1 + \dot{m}_1/\dot{m}_o) p_o M_o \sqrt{2 + (\gamma - 1)M_o^2} (1 - \delta^*/\delta)_o} , \tag{4}$$

$$G = \frac{(p_1 - p_{sep})/p_o - \gamma M_{sep}^2 p_{sep}/p_o (1 - \delta^*/\delta - \theta/\delta)_{sep}}{p_1/p_o - 1 - \gamma M_o^2 (1 - \delta^*/\delta - \theta/\delta)_o - \dot{I}_1/(p_o \delta_o) + \tau_w \hat{s}/(p_o \delta_o)} \tag{5}$$

where $\dot{m}_1 = 0.03(\rho u)_1 \hat{s}[(\delta_o - \delta_o^*)/\theta_o - 3]^{-0.62}$, (6)

$$\dot{I}_1/(p_o \delta_o) = \dot{m}_1/\dot{m}_o (1 - \delta^*/\delta)_o \gamma M_o M_1 \sqrt{\frac{2 + (\gamma - 1)M_o^2}{2 + (\gamma - 1)M_1^2}} , \tag{7}$$

and $$p_1 = 1/\hat{s}_{sep} \int_{\hat{s}_o}^{\hat{s}_{sep}} p_\ell d\hat{s} \tag{8}$$

This method uses the control volume approach. The control volume consists of a section of the boundary layer with one end at the minimum static pressure location and the other at the separation location. Quantities with a subscript of 1 are conditions at the

outer edge of the control volume. Equations 4 and 5 are equations for the ratio of the boundary-layer thickness at the minimum static pressure location to that at the separation location. Equation 4 is an integrated form of the continuity equation, while equation 5 is an integrated form of the momentum equation. Flow separation occurs when

$$F = G \tag{9}$$

The Stratford criterion is a well-known method for determining the separation location (refs. 36 and 38). Several similar existing methods were combined to form this criterion. Lahti's version of this criterion was used in this evaluation:

$$\bar{C}_{p,sep} \left(\bar{s} \frac{d\bar{C}_p}{d\bar{s}} \right)_{sep}^{0.5} (10^{-6} N_{Re})_{sep}^{-0.1} = C \tag{10}$$

where $\bar{C}_p = 1 - \left(\frac{M_\ell}{M_o} \right)^2$, (11)

and $\bar{s} = \hat{s} - \hat{s}_o + s_{fs}$ (12)

The effect of the forebody pressure distribution and the actual boundary layer transition location on the boundary layer flow over the boattail is handled by computing the distance to a fictitious stagnation point s_{fs} (the effective distance for a flat-plate turbulent boundary layer to develop the momentum thickness at $\hat{s}_o$). Separation is indicated when the value of C is between 0.5 and 0.6. The separation location corresponds to the maximum value of C in

this interval. This criterion assumes that the boundary layer consists of two different layers. The inner one is independent of upstream conditions, and the outer layer is assumed to be affected by only the initial velocity profile and the downstream pressure gradient.

The Townshend criterion is given by the equation (refs. 39 and 52):

$$\text{Log}\left[\frac{u_o}{\nu}\left(\frac{d\hat{s}}{d\hat{C}_p}\right)_{ps} C_{f,o}^{1.5}\right] = \left(\frac{1}{2.98}\,\frac{\hat{C}_{p,sep}}{C_{f,o}} + 2.7\right)^{0.5}$$

$$+ \text{Log}\left[\left(\frac{1}{2.98}\,\frac{\hat{C}_{p,sep}}{C_{f,o}} + 2.7\right)^{0.5} - 1\right] - 2.913 \qquad (13)$$

It is derived with the assumption that the separation is dependent upon the pressure gradient. This is incorporated into the criterion by the presence of the pressure gradient upstream of separation.

The Angle method is given by the following equation:

$$M_{sep} \sin \beta_{sep} = -0.247 \qquad (14)$$

It assumes that the separation location is a function of the local boattail angle β and Mach number. It was derived by fitting a curve to this set of experimental data.

The Goldschmied criterion is another well-known simple method (refs. 40 and 41):

$$\hat{C}_{p,sep} = 200\ C_{f,o} \tag{15}$$

It assumes that the boundary layer consists of two layers. It also assumes that a line of constant total pressure exists parallel to the surface. This line intersects the inner layer at the beginning of the adverse pressure gradient. Separation is assumed to occur when the laminar sublayer thickens enough to intersect the line of constant total pressure. This viscous phenomenon is correlated through the use of the skin friction coefficient at the start of the adverse pressure gradient.

The Wu criterion is another simple equation (ref. 51):

$$\frac{p_{sep}}{p_o} - 0.565\ M_o = 0.795 \tag{16}$$

It is based on experimental data, and assumes that separation is a function of two parameters. One of these is the Mach number at the start of the adverse pressure gradient. The other is the ratio of the separation static pressure to the minimum static pressure.

These eight criteria were tested by comparing their separation predictions with experimental data. The cases used in the evaluation were the conditions for which separation was observed on the configurations with solid simulators. Figures 14 and 15 show the variation of separation location with Mach number for the various

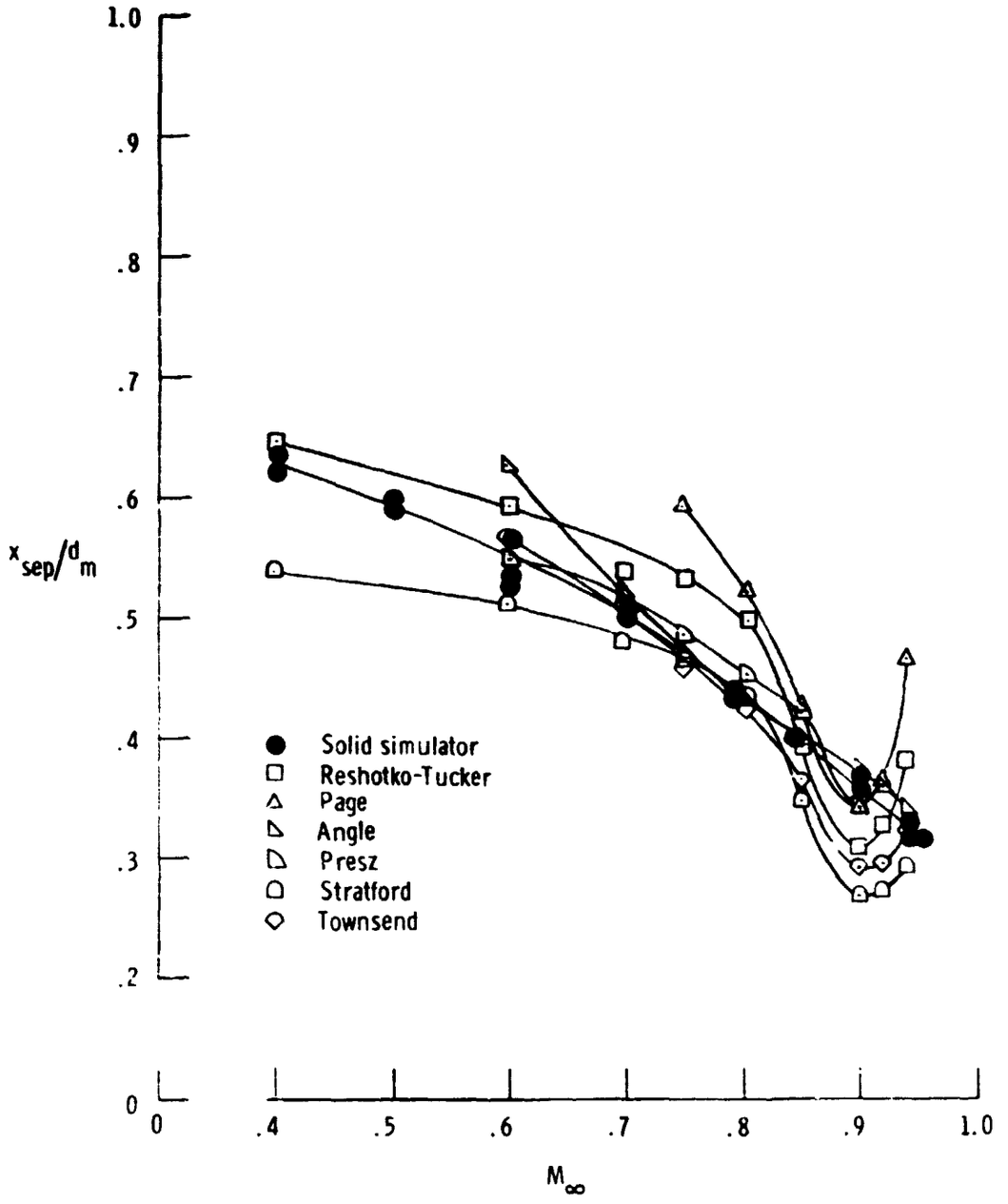

(a) Configuration 1 (l/d_m = 0.80, d_e/d_m = 0.50)

Figure 14.- Comparison of the variation of separation location predicted by various methods with Mach number for configurations with solid plume simulators. Experimental pressure distributions used in predicting separation locations.

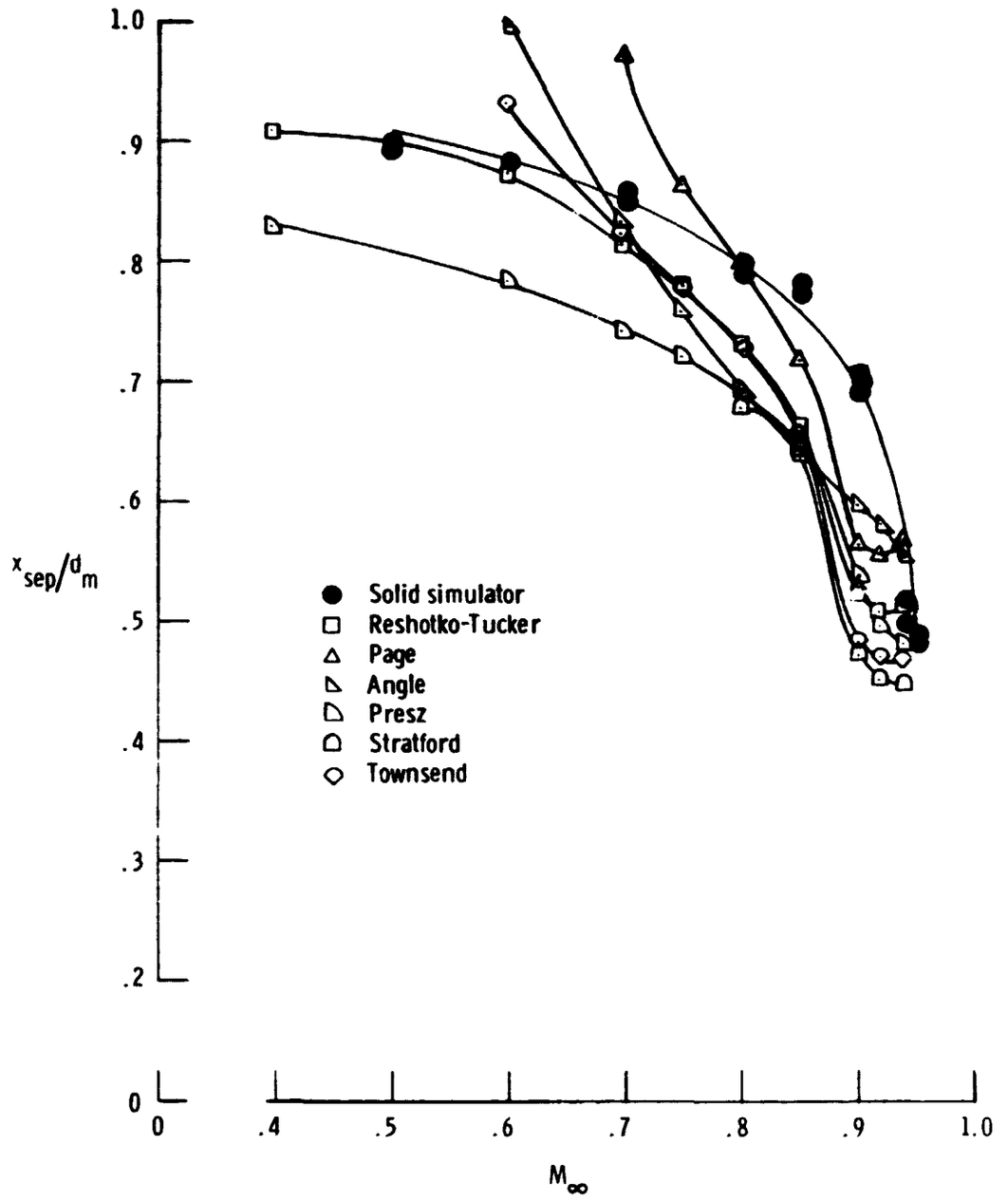

(b) Configuration 2 (ι/d_m = 1.0, d_e/d_m = 0.50)

Figure 14. - Continued.

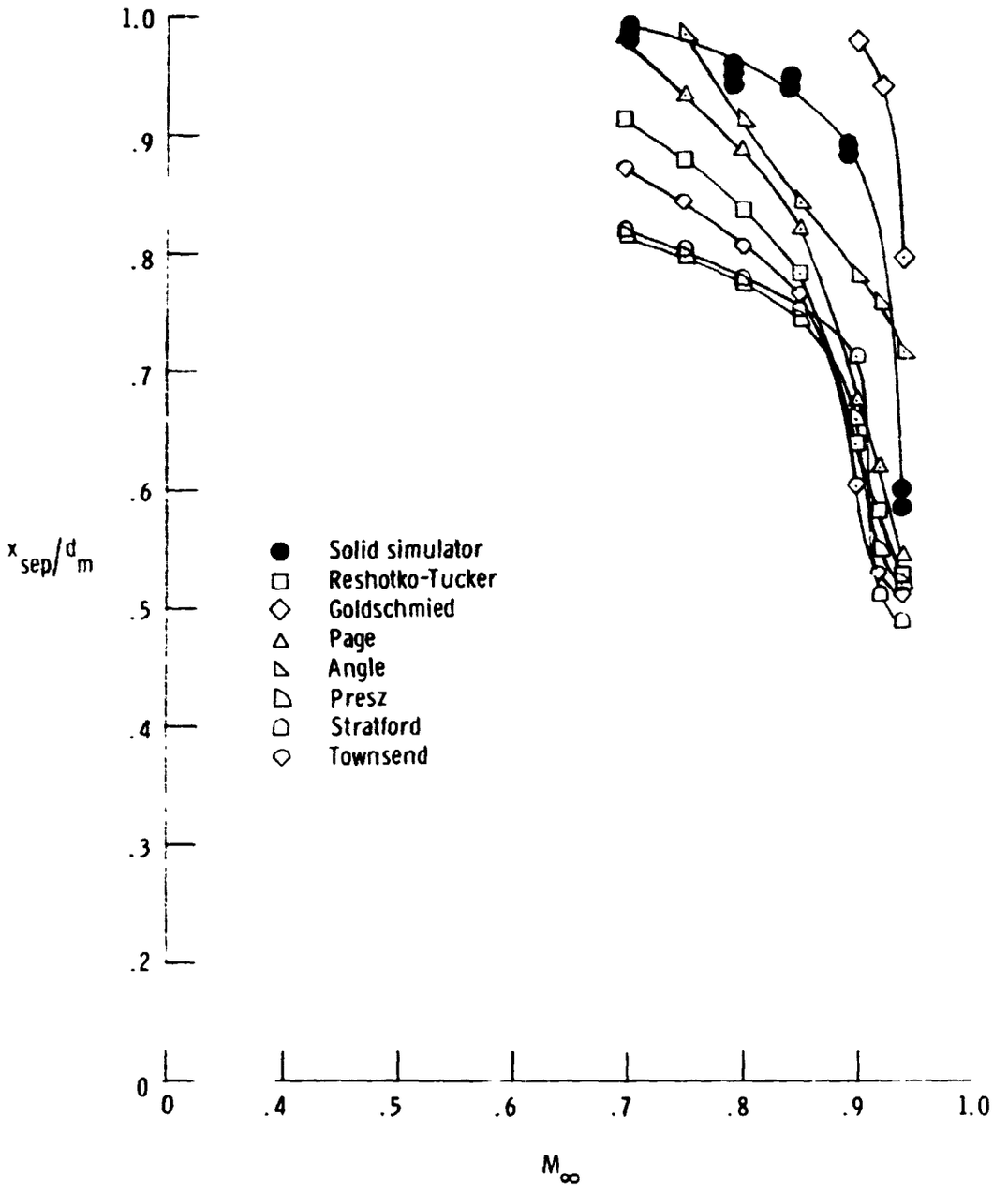

(c) Configuration 4 (ℓ/d_m = 1.0, d_e/d_m = 0.60)

Figure 14. - Continued.

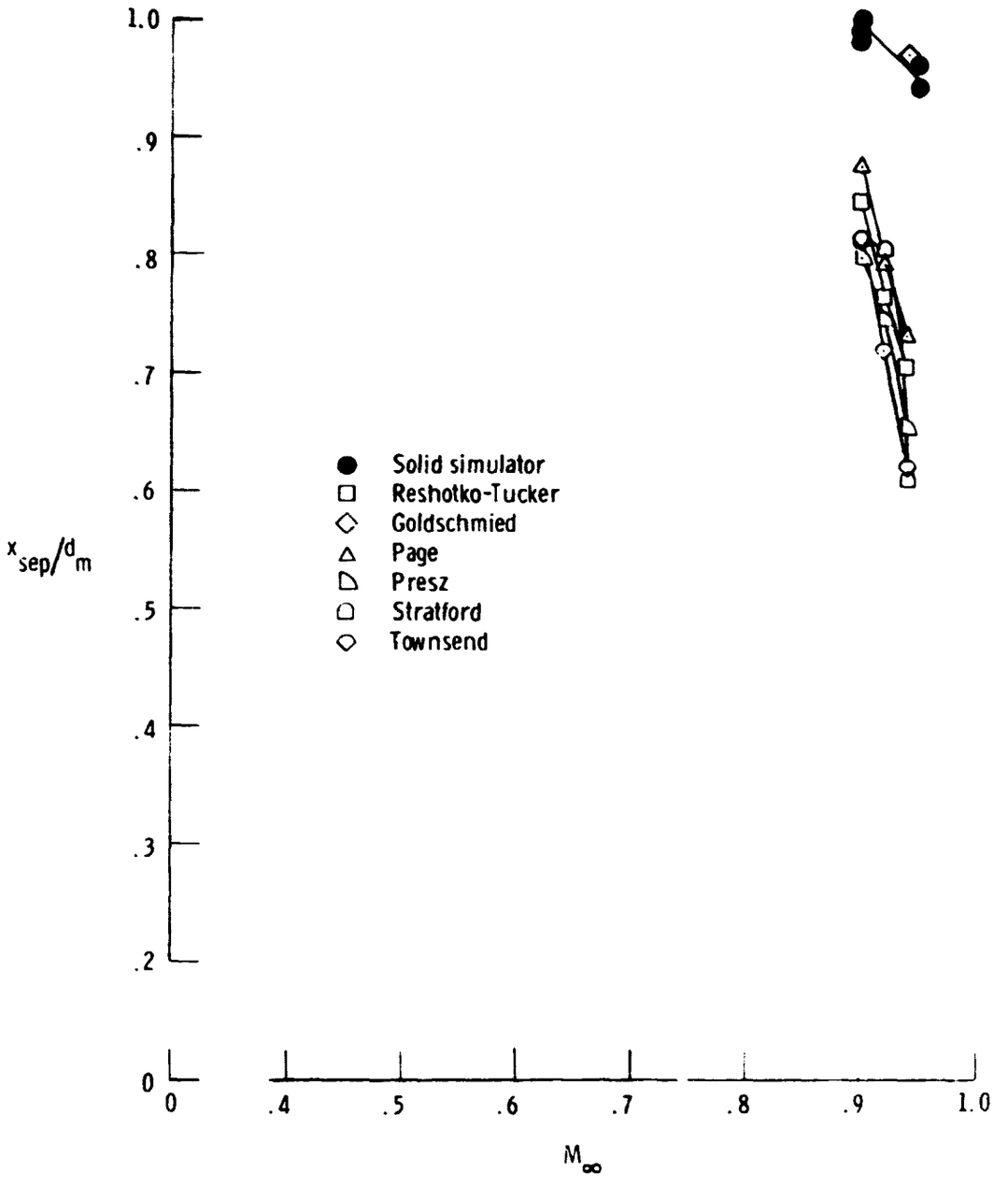

(c) Configuration 6 ($\iota/d_m = 1.0$, $d_e/d_m = 0.70$)

Figure 14. - Concluded.

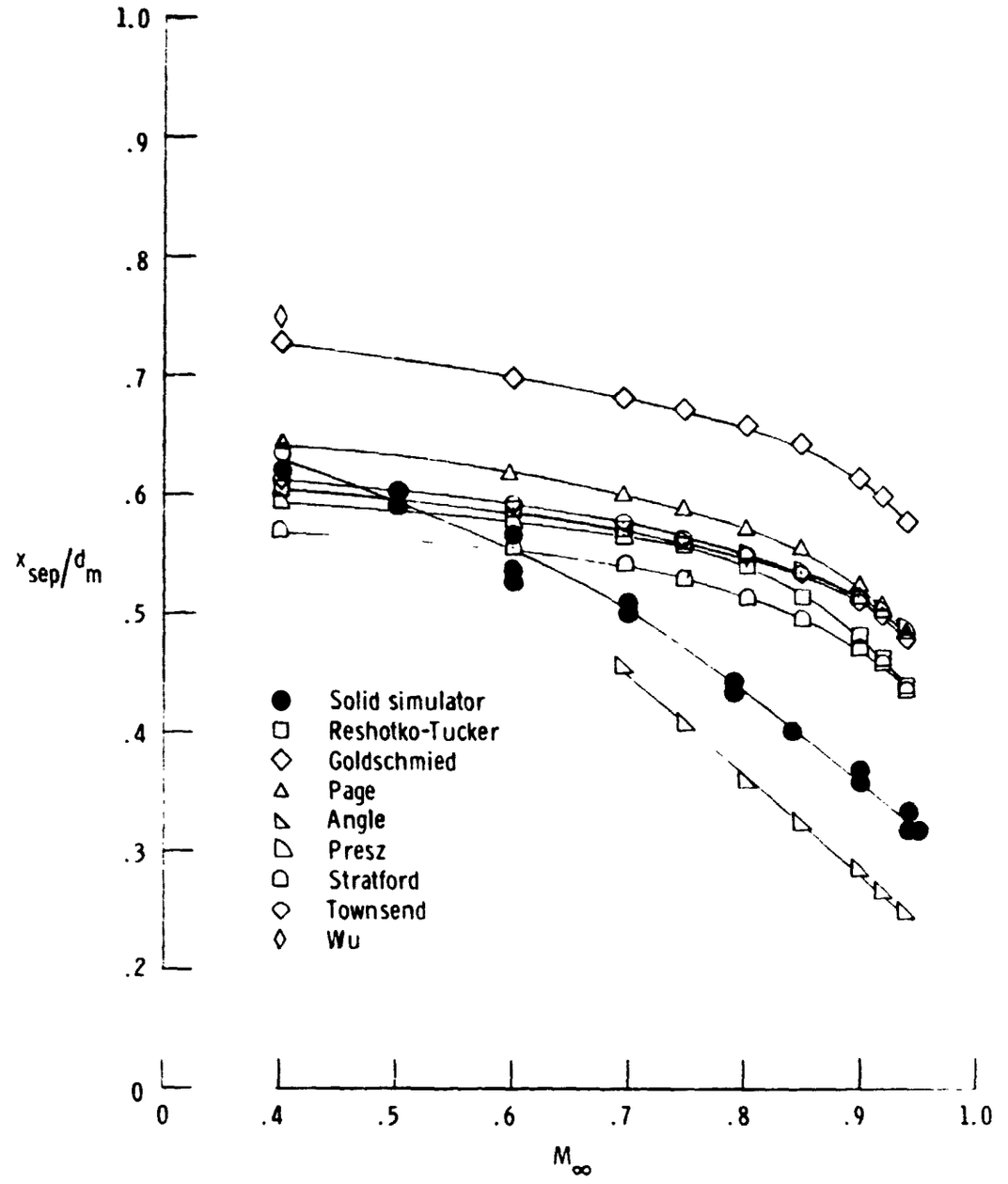

(a) Configuration 1 (l/d_m = 0.80, d_e/d_m = 0.50)

Figure 15.- Comparison of the variation of separation location predicted by various methods with Mach number for configurations with solid plume simulators. Theoretical inviscid pressure distributions used in predicting separation locations.

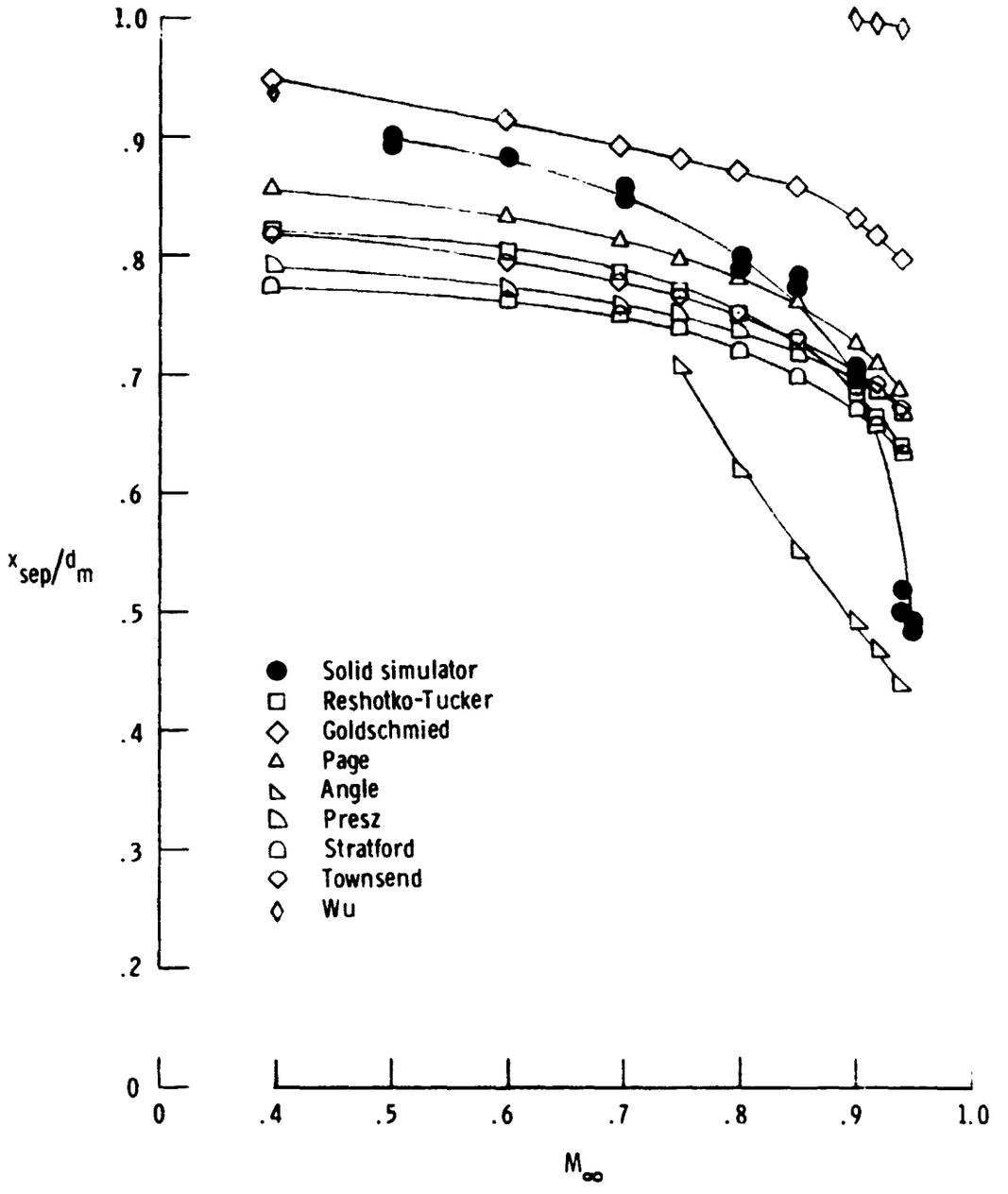

(b) Configuration 2 (ι/d_m = 1.0, d_e/d_m = 0.50)

Figure 15. - Continued.

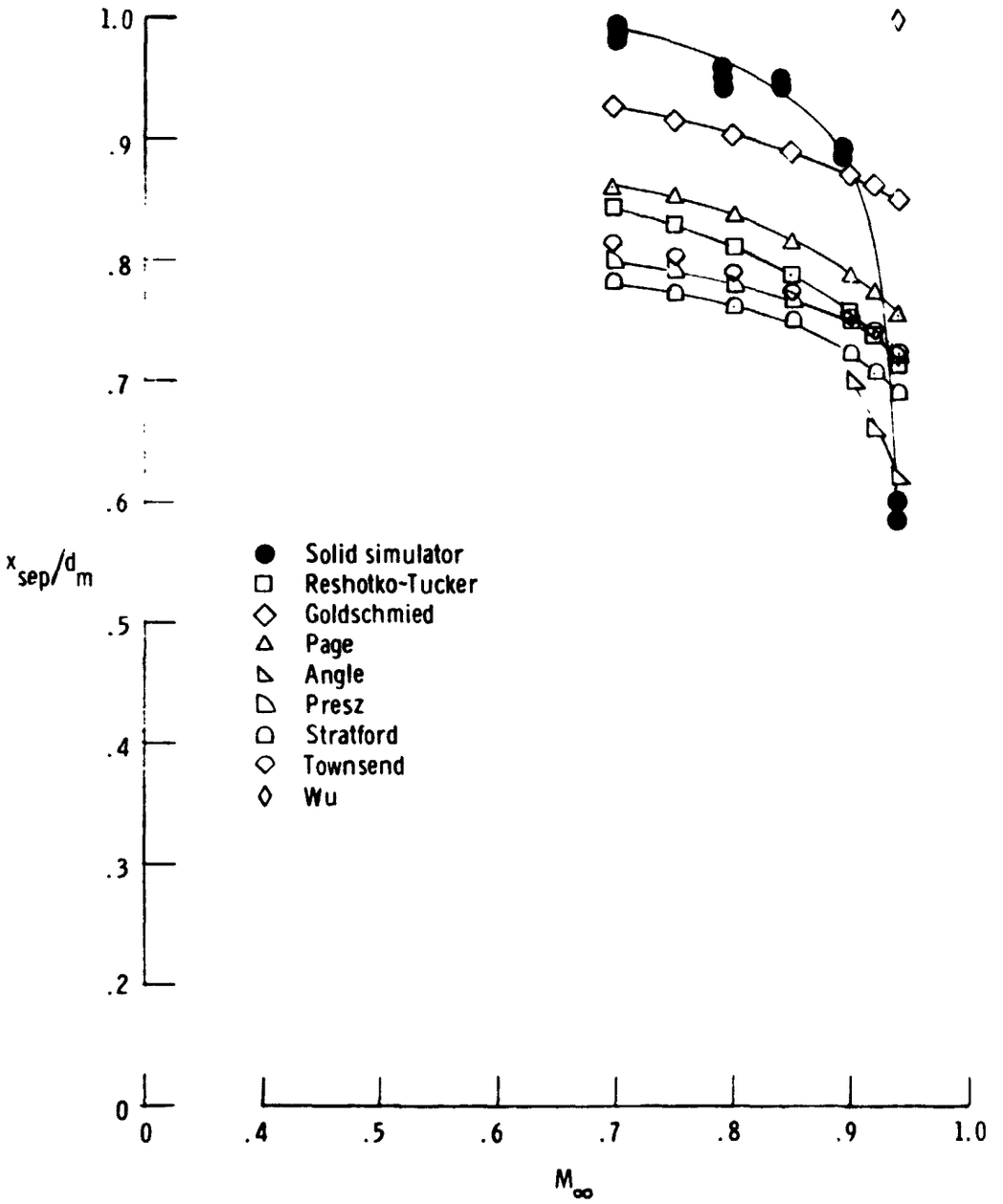

(c) Configuration 4 (ι/d_m = 1.0, d_e/d_m = 0.60)

Figure 15. -Continued.

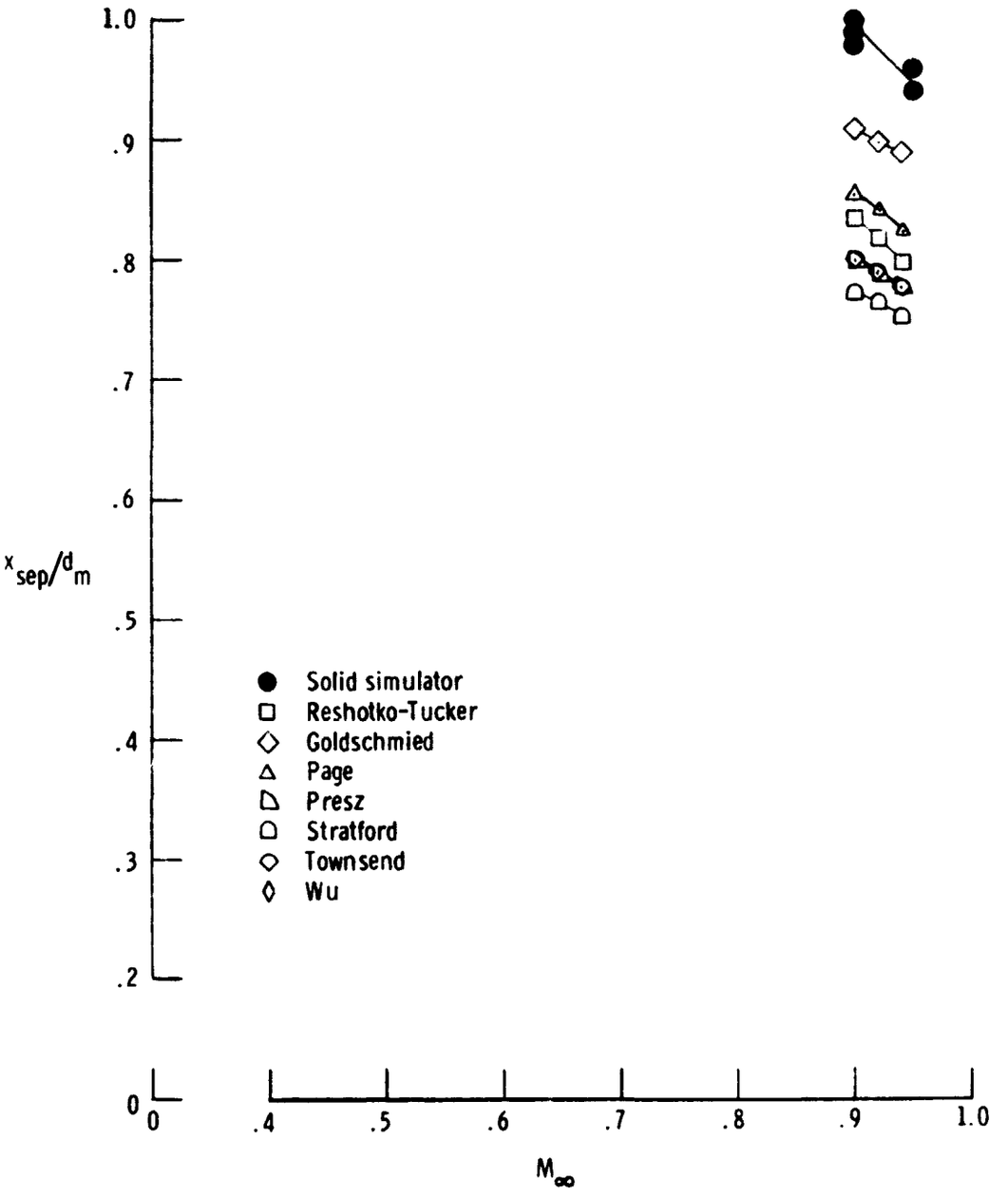

(d) Configuration 6 (ι/d_m = 1.0, d_e/d_m = 0.70)

Figure 15. -Concluded.

methods. In figure 14, the experimental pressure distributions were used in the calculations. In figure 15, the theoretical inviscid pressure distributions were used. The scatter in the experimental data caused much of the scatter in figure 14. Also, because of the pressure plateau in the separated region, a small error in the value of the predicted separation pressure can result in a large error in separation location when using experimental pressures. In fact, the Goldschmied criterion predicted separation for only four cases, and the Wu criterion failed to predict any at all. As shown in figure 15, the predicted trends using the inviscid pressure distributions were much smoother, although they were often very inaccurate. The Wu criterion was only able to predict separation for five cases. In general when the inviscid pressure distribution was used, the Goldschmied criterion predicted the most rearward separation locations. It was followed in order by the predictions of Page, Reshotko-Tucker, Townshend, Presz, and Stratford. The best overall predictions were made using the Angle criterion based on experimental pressure distributions. This was not surprising since the same data were used to derive this criterion. However, none of the criteria appeared to provide very accurate results.

This inaccuracy is better seen in figures 16 and 17. In figure 16, the predicted separation locations obtained using the experimental pressure distributions are plotted versus the experimental separation locations. In figure 17, the predictions obtained using the inviscid pressure distributions are plotted. (The limited results of the Wu

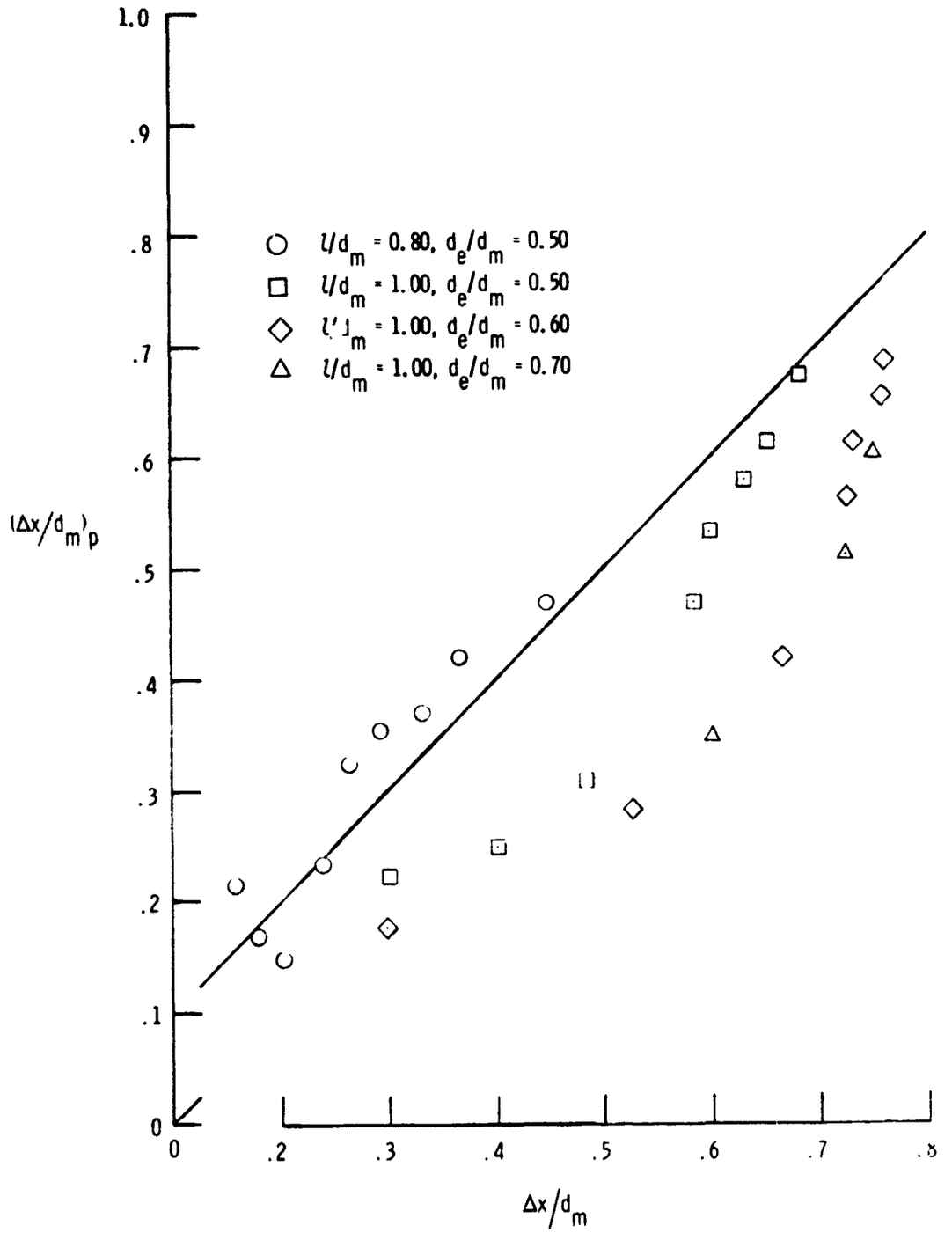

(a) Reshotko-Tucker

Figure 16.- Evaluation of predicted separation locations with oil-flow data for configurations with solid plume simulators. Experimental pressure distributions used in predicting separation locations.

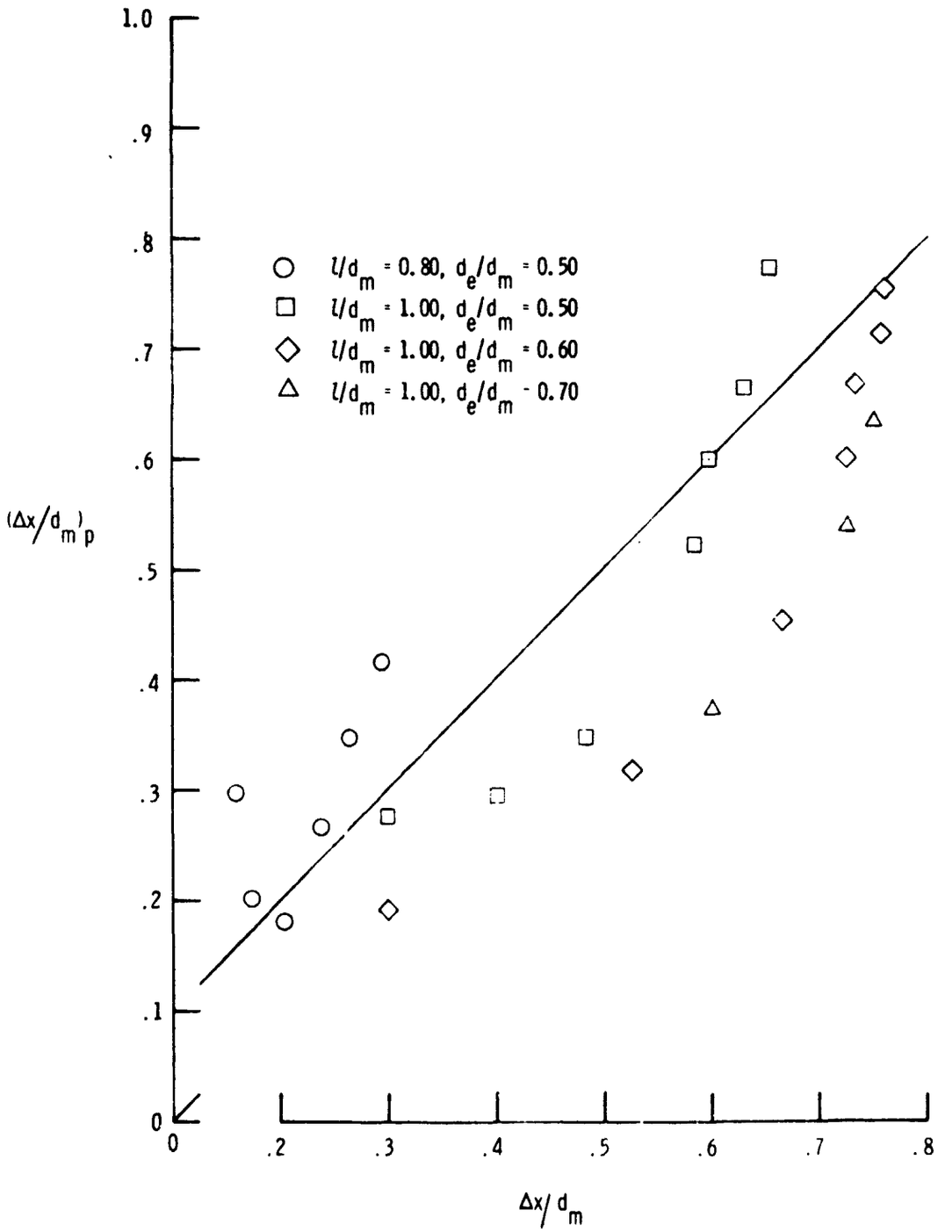

(b) Page

Figure 16. -Continued.

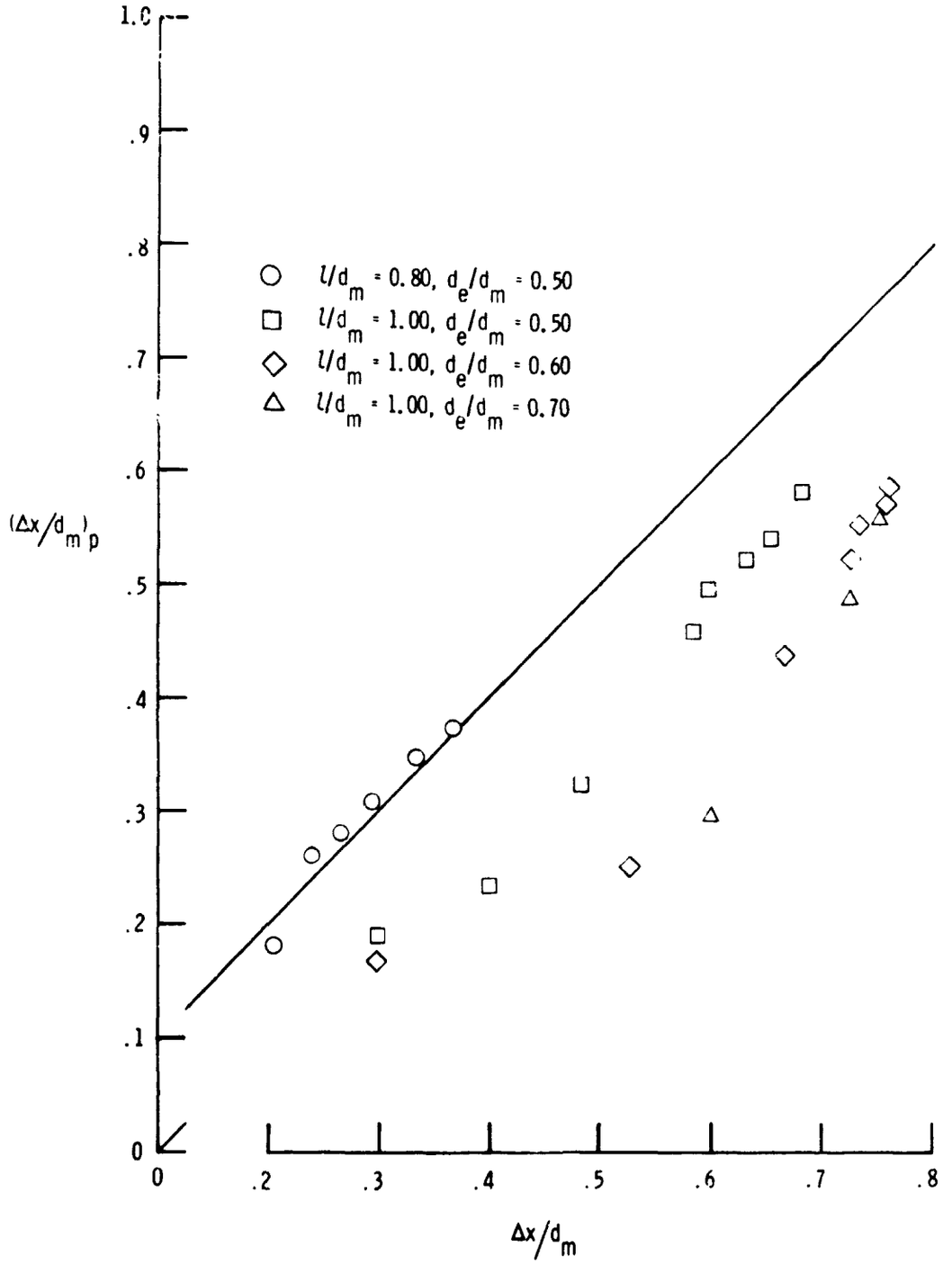

(c) Presz

Figure 16. -Continued.

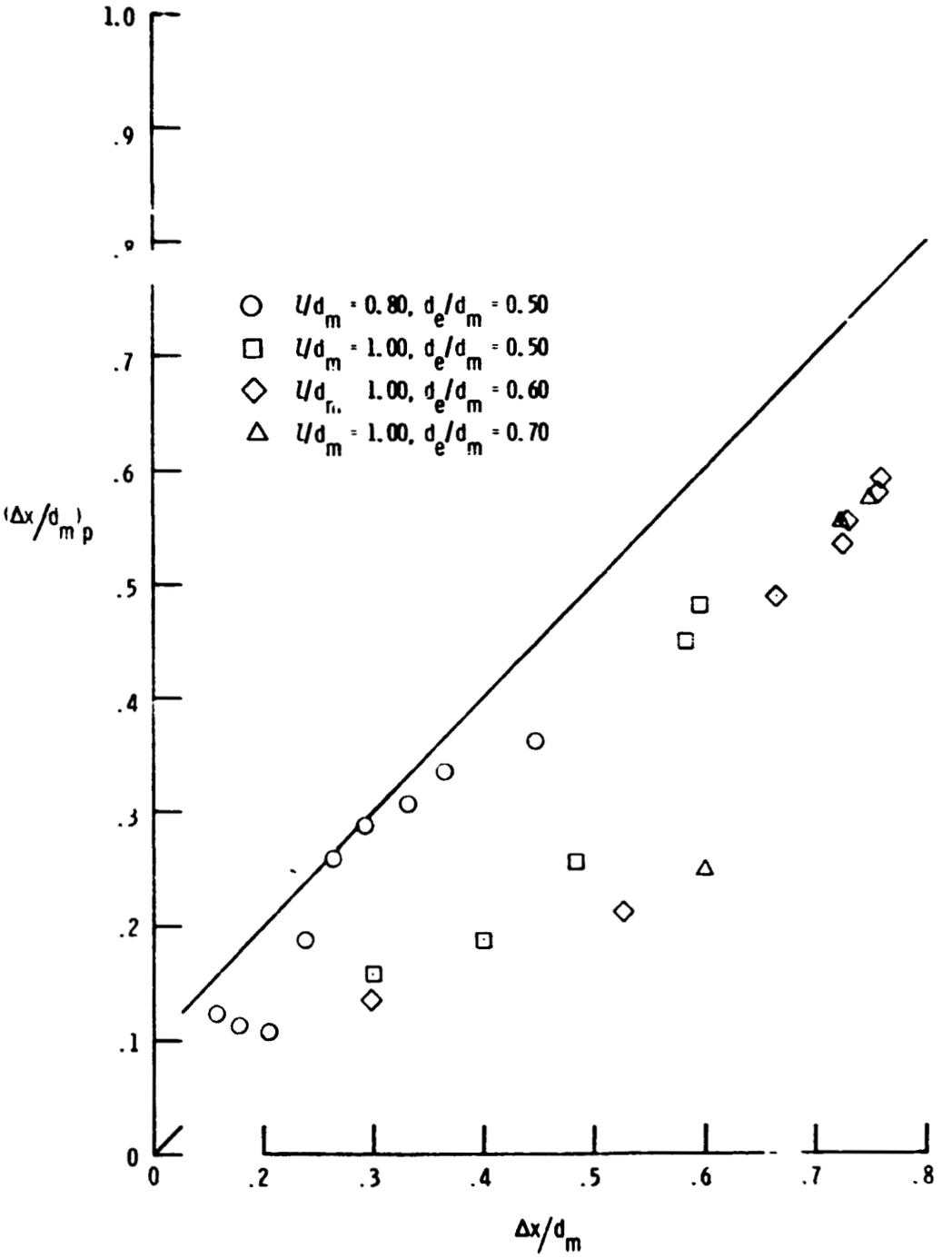

(d) Stratford

Figure 16. -Continued.

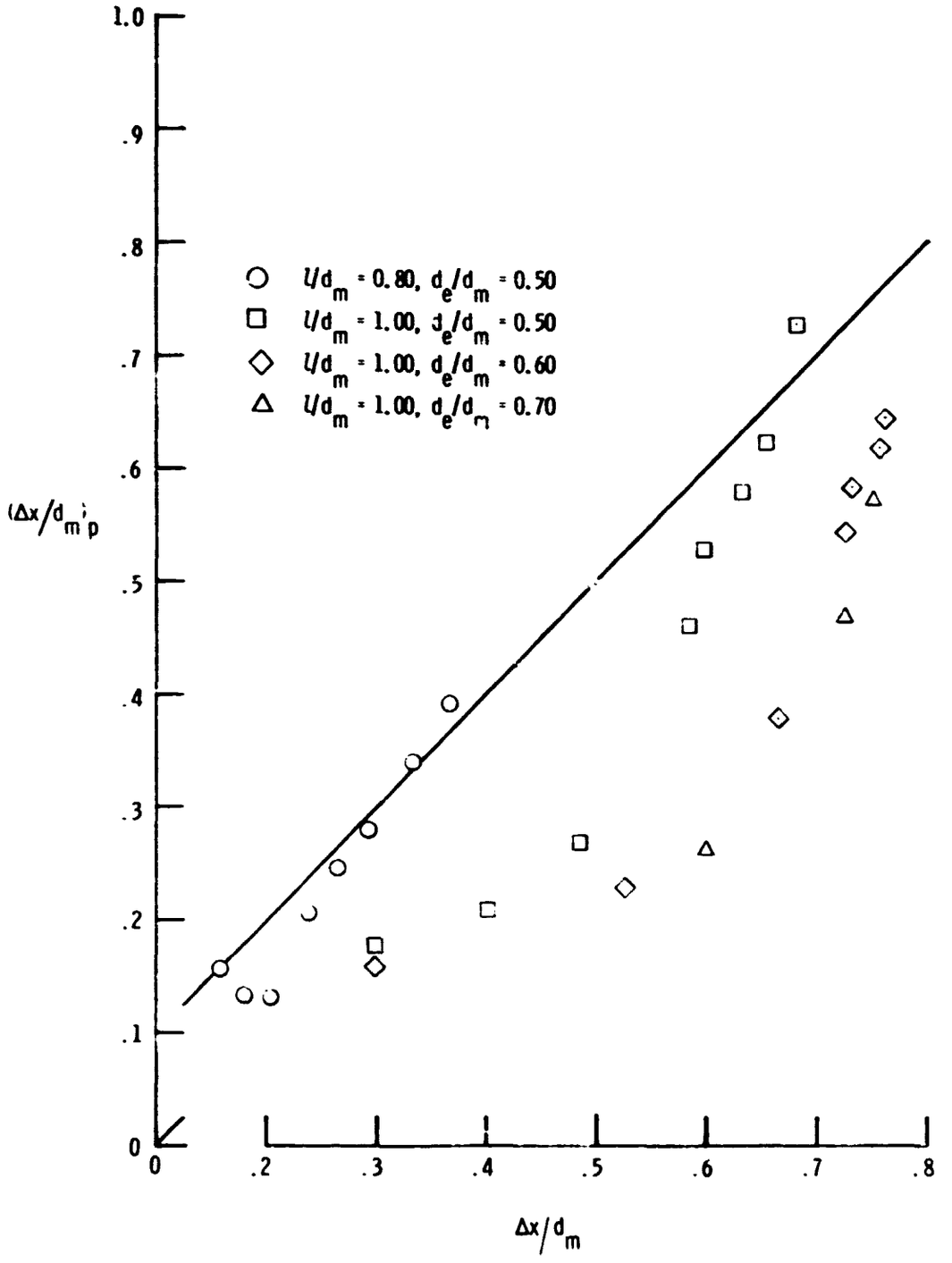

(e) Townsend

Figure 16. -Continued.

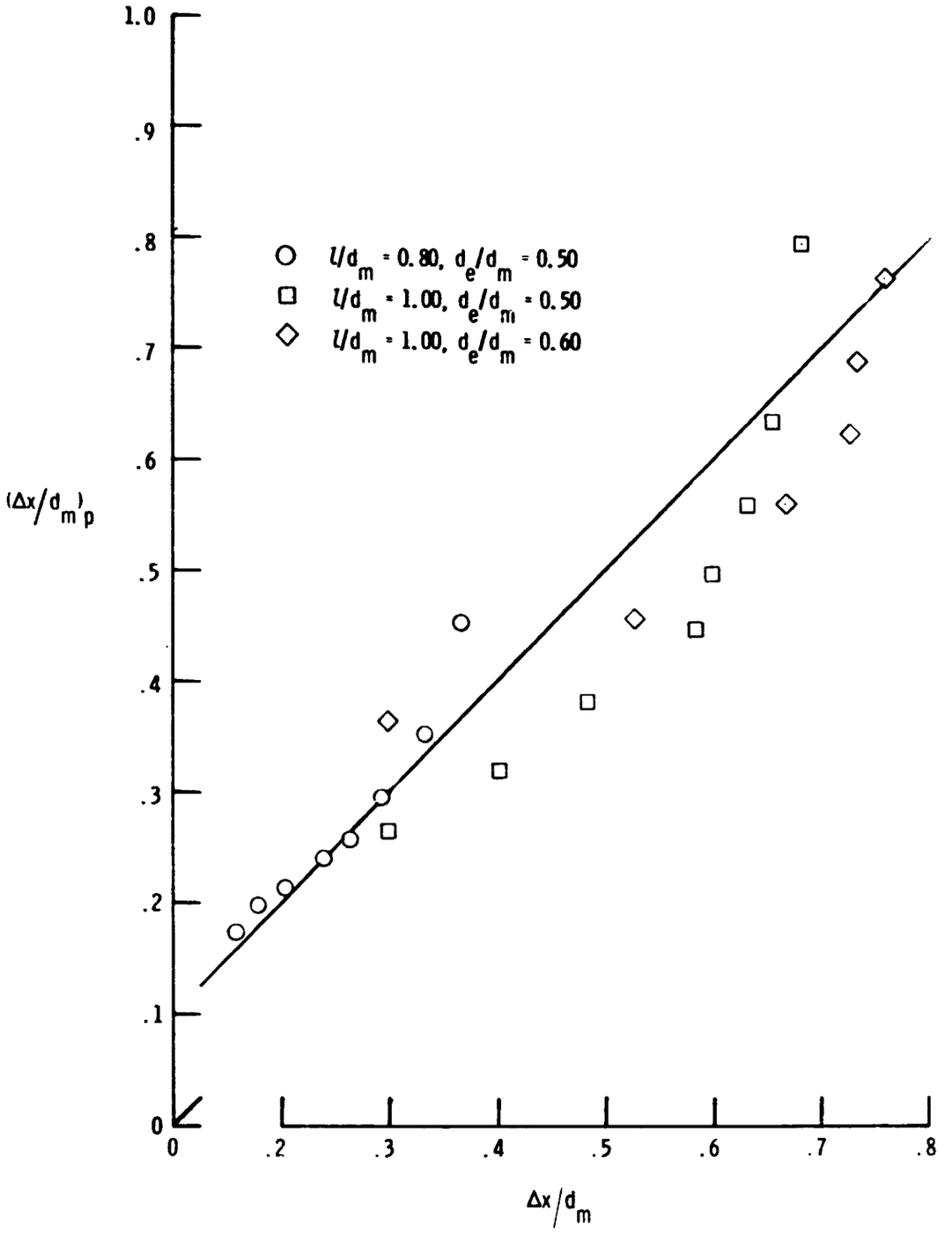

(f) Angle

Figure 16. -Concluded.

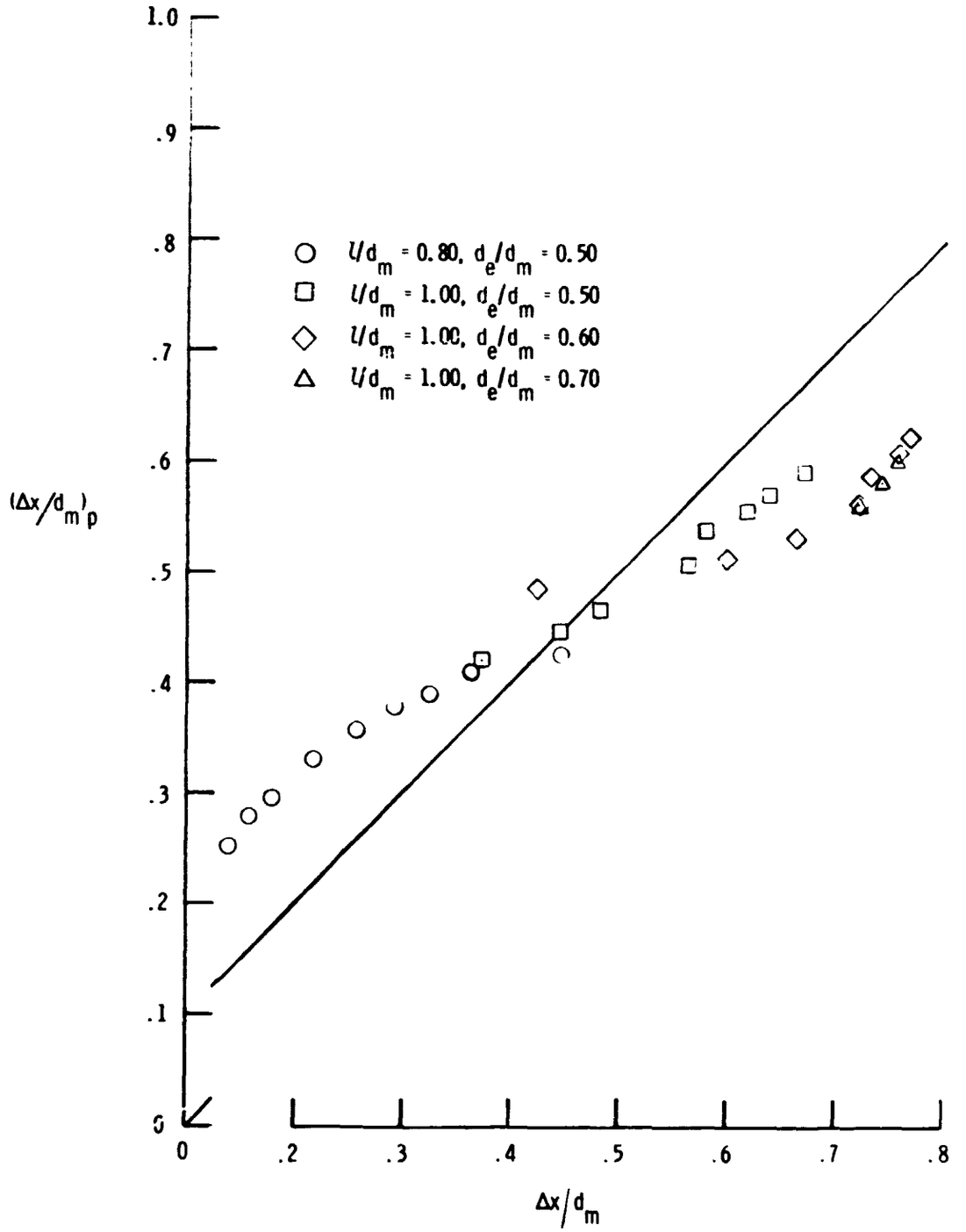

(a) Reshotko-Tucker

Figure 17. -Evaluation of predicted separation locations with oil-flow data for configurations with solid plume simulators. Theoretical inviscid pressure distributions used in predicting separation locations.

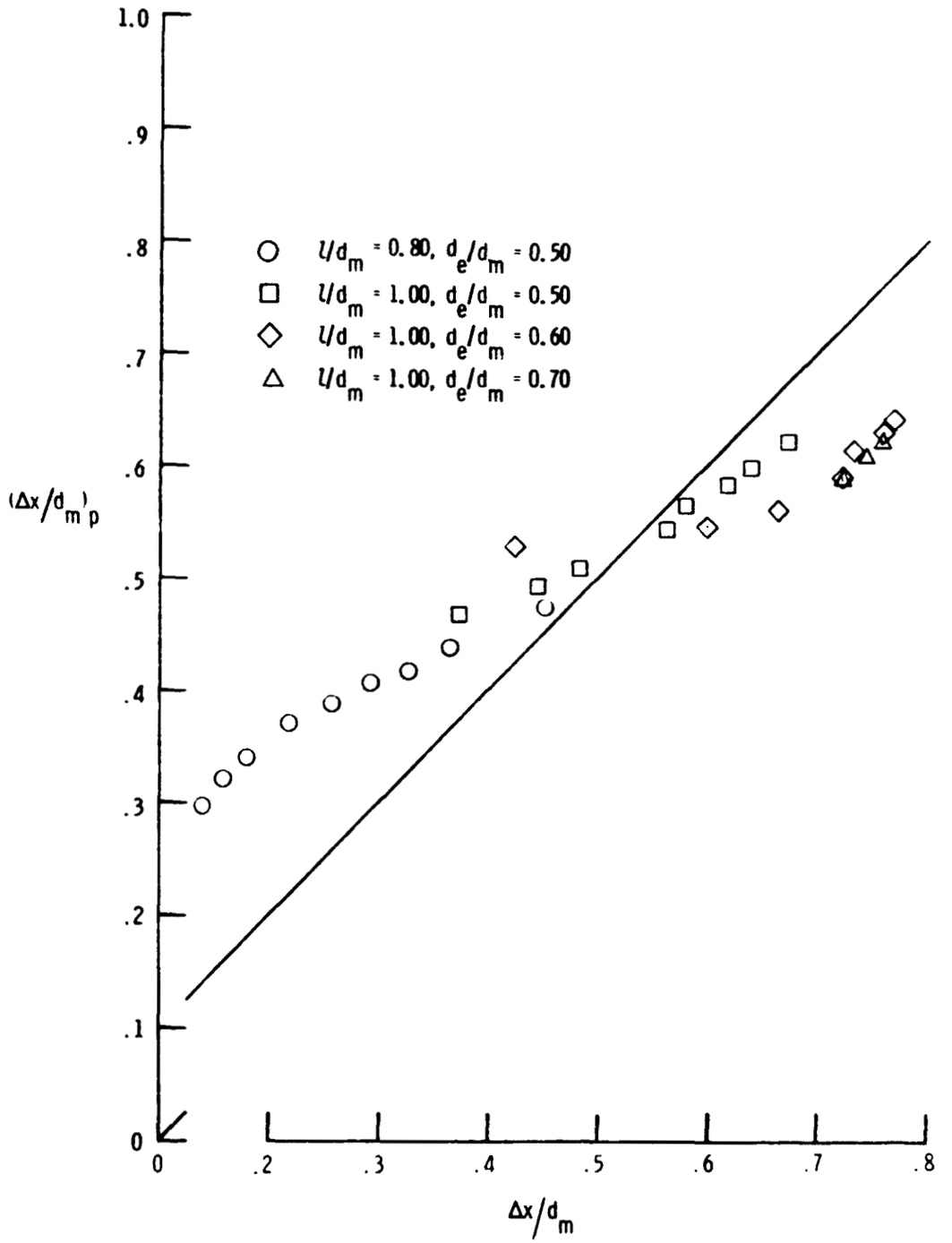

(b) Page

Figure 17. -Continued.

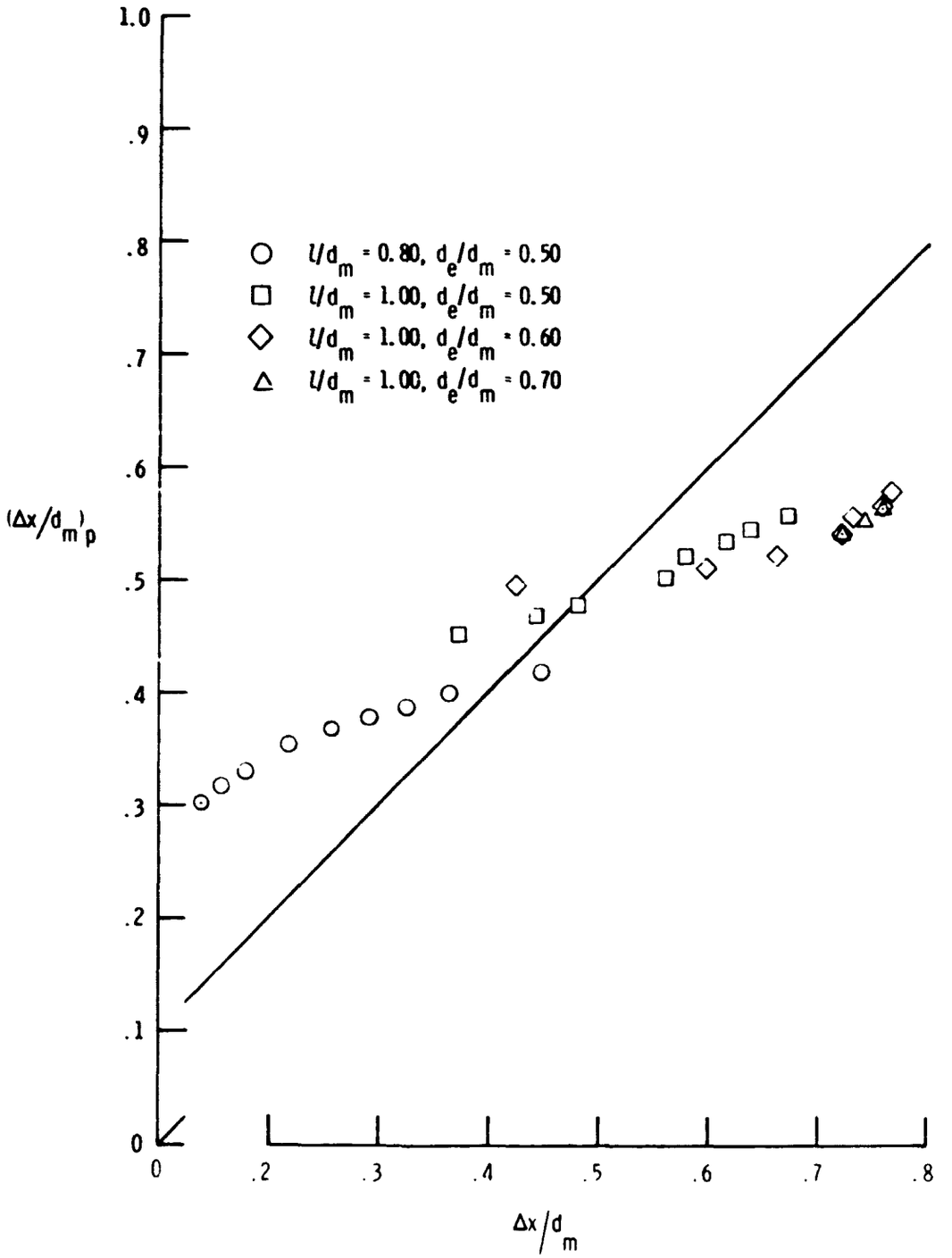

(c) Presz

Figure 17. -Continued.

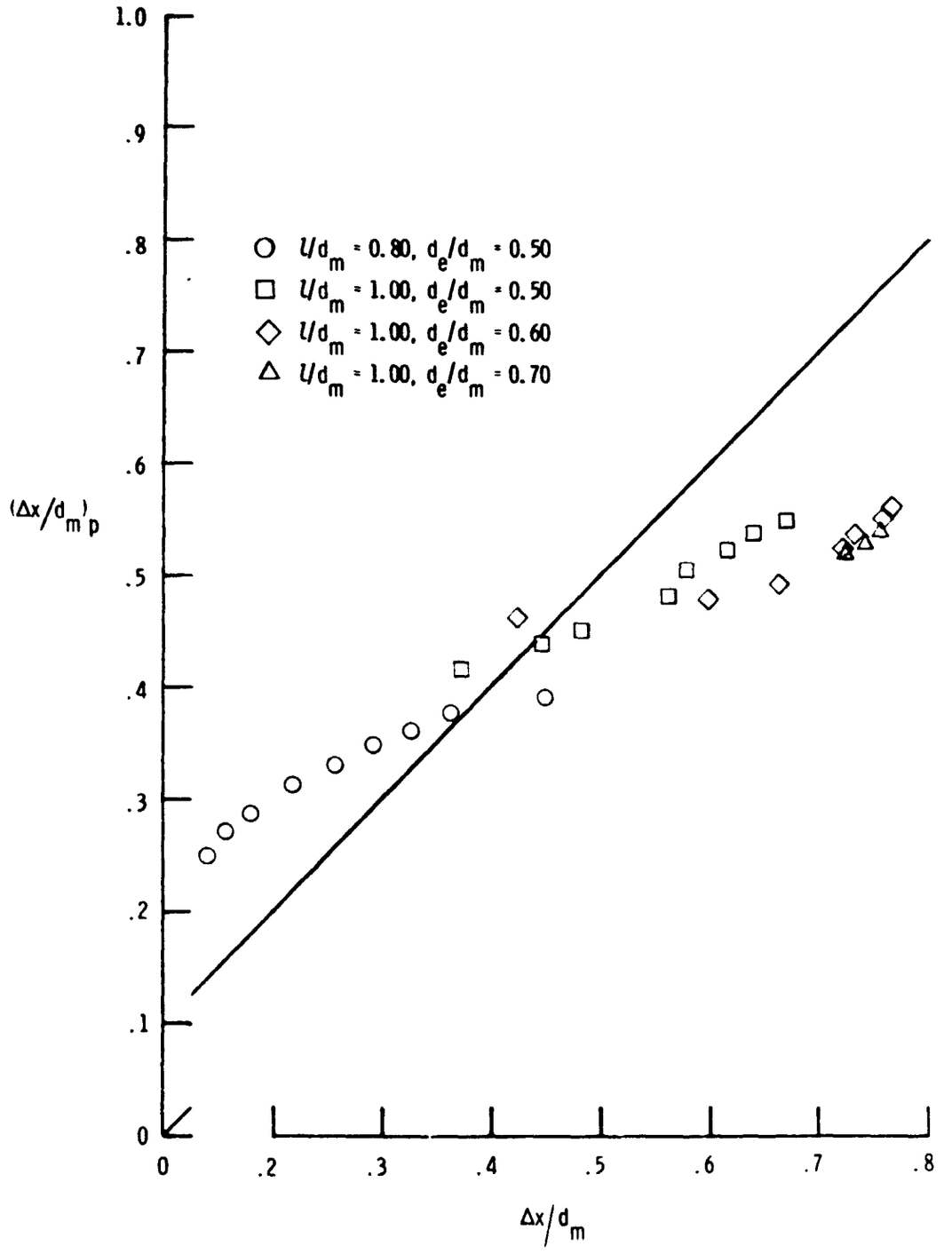

(d) Stratford

Figure 17. -Continued.

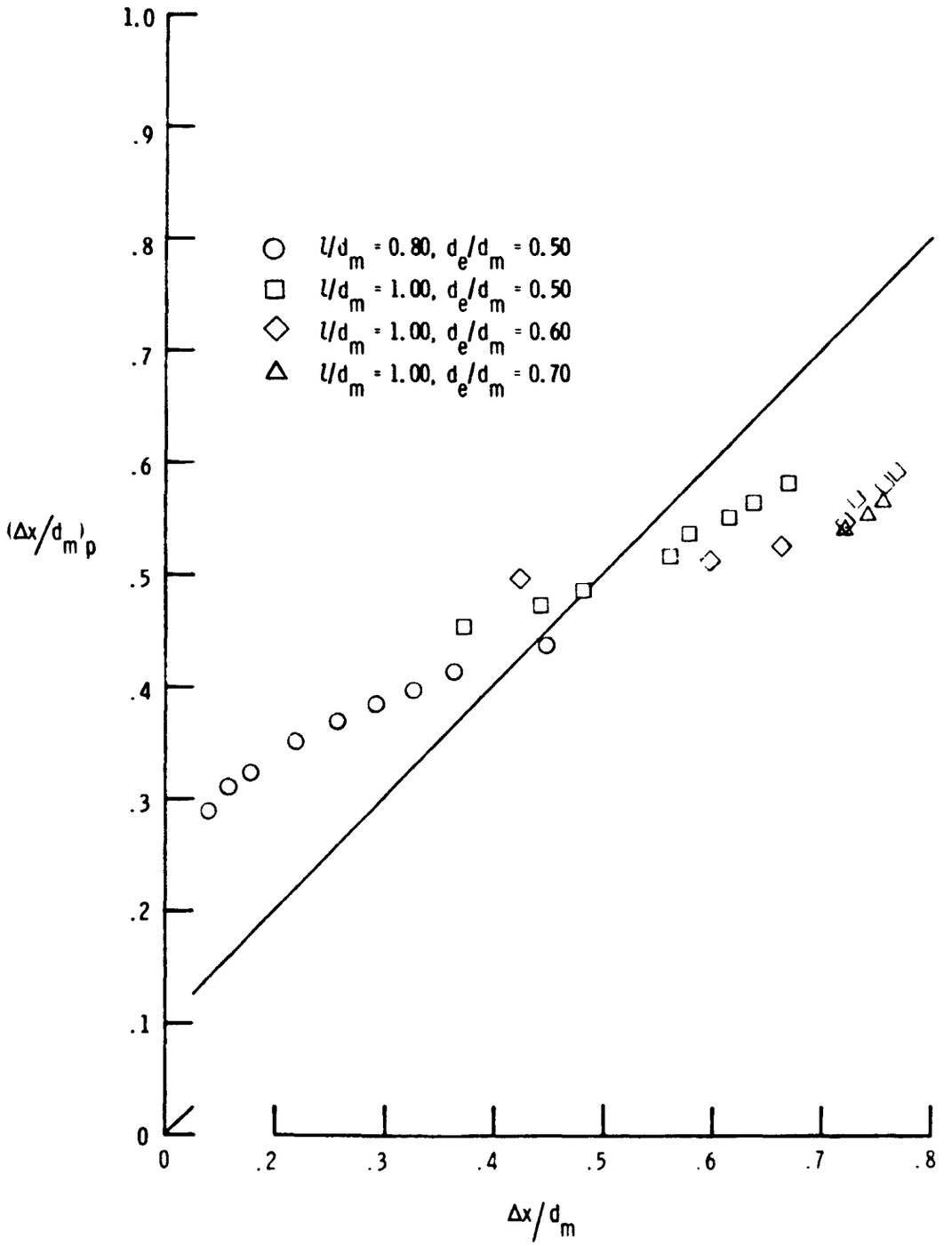

(e) Townsend

Figure 17. -Continued.

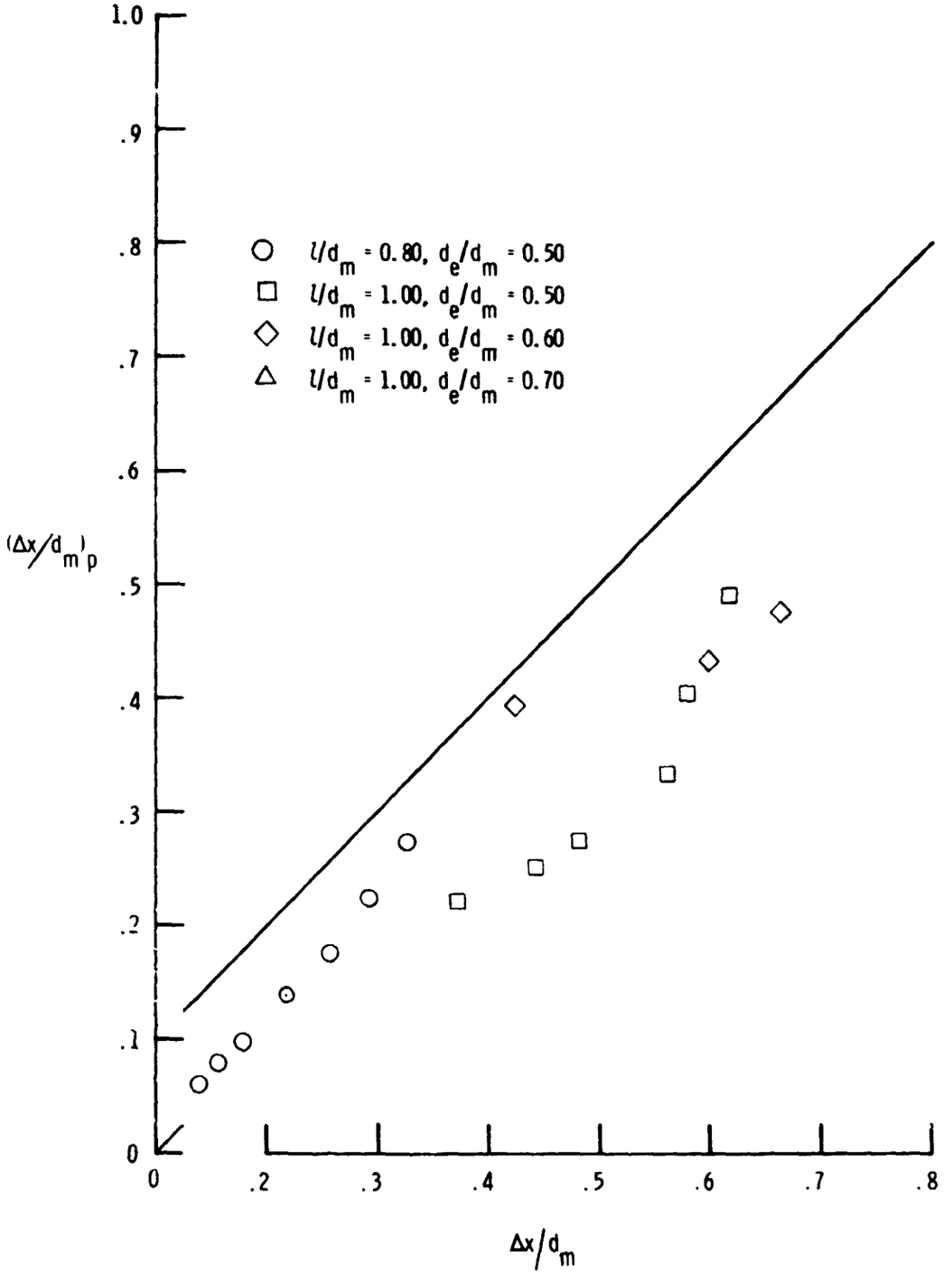

(f) Angle

Figure 17. -Continued.

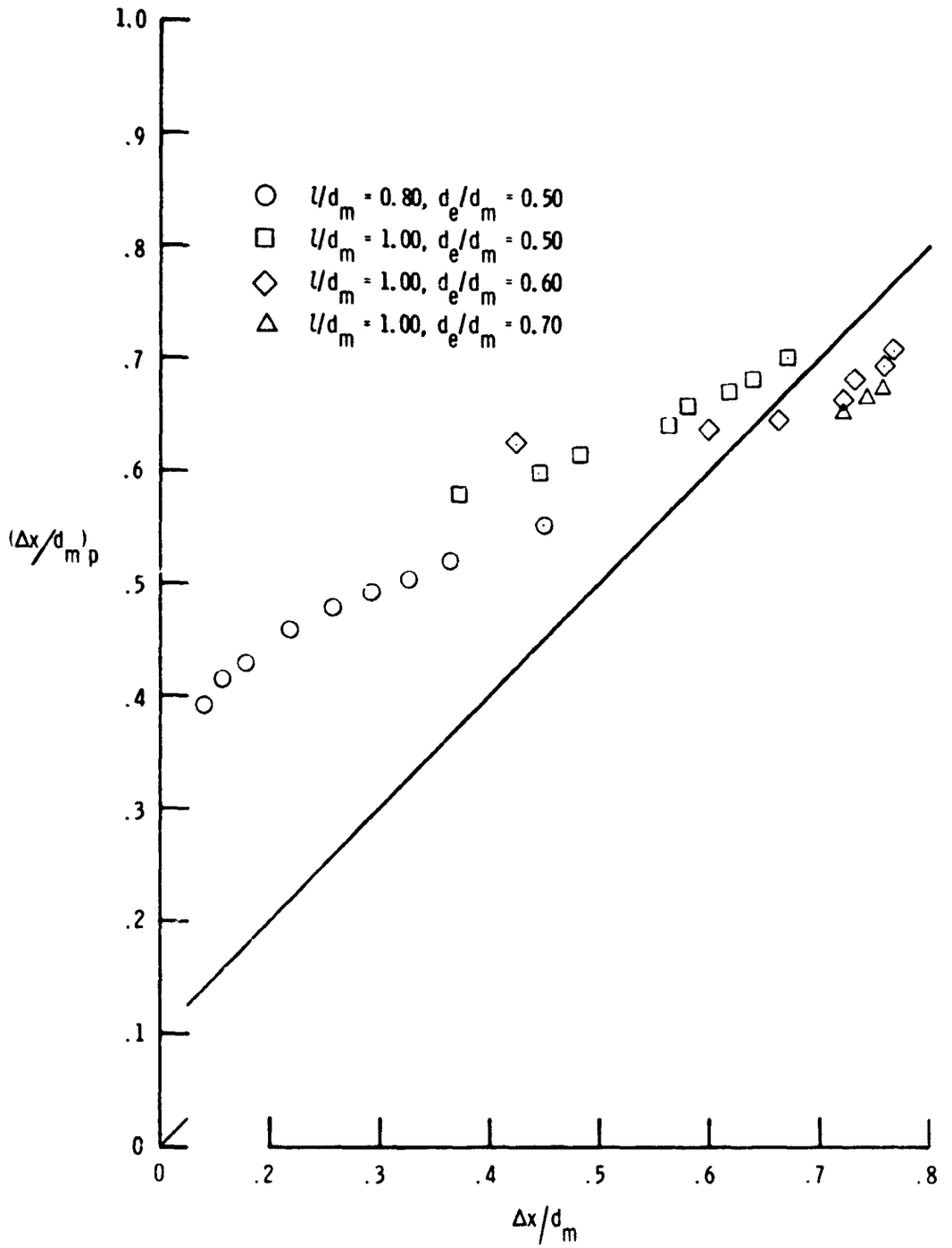

(g) Goldschmied

Figure 17. -Concluded.

criterion and the Goldschmied criterion based on the experimental pressure distributions are not presented.) The extent that the predictions deviate can be seen for all methods. It should be noted, however, that some of the scatter seen in both figures is due to the experimental error in the oil-flow data itself. By comparing the standard error of estimate for each criterion,

$$E = \sqrt{\sum_{i}^{n} \frac{[y_i - (a + bz_i)]^2}{n - 2}} \qquad (17)$$

it was found that the Angle method based on the experimental pressure distributions yielded the best results (E = 0.073). The next best results were obtained by using the Reshotko-Tucker criterion based on the inviscid pressure distributions.

It is also seen in figures 16 and 17 that the results using the inviscid pressure distributions are more linear. By fitting a least squares curve, i.e. by treating the predictions as a linear function of the experimental data, an improved prediction can empirically be obtained. The standard errors of estimate of the resulting curve fits are as follows:

Reshotko-Tucker	-	E = 0.038,
Page	-	E = 0.041,
Presz	-	E = 0.047,
Stratford	-	E = 0.048,
Townshend	-	E = 0.051,
Angle	-	E = 0.058,
Goldschmied	-	E = 0.062.

The improved results obtained by applying the curve fit to the Reshotko-Tucker criterion are compared with the oil-flow data in figure 18. The

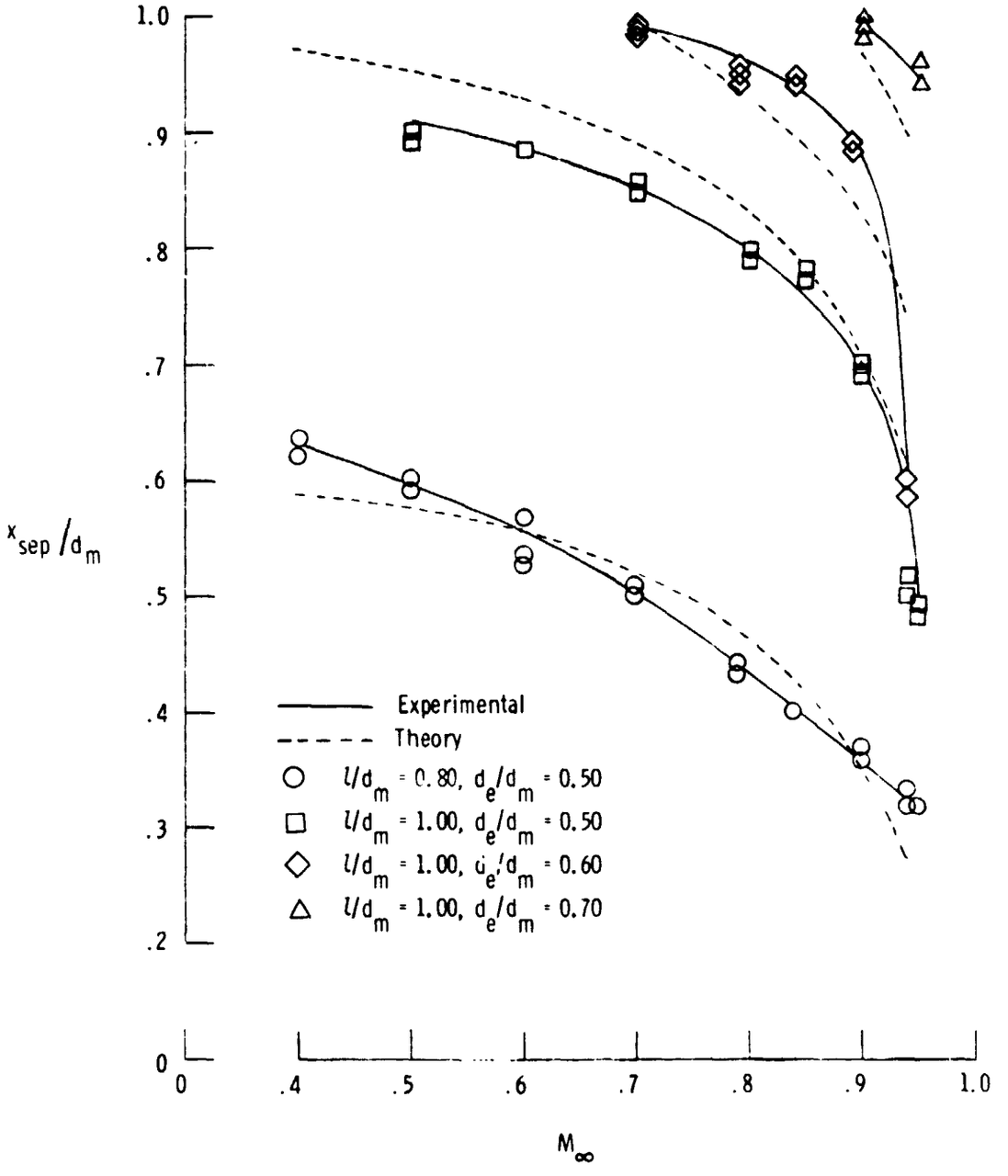

Figure 18. -Comparison of oil-flow data and predicted separation locations made using least squares curve fit applied to Reshotko-Tucker criterion.

least squares equation for this criterion is:

$$\frac{x_{sep}}{d_m} = 1.870 \frac{x_{sep,p}}{d_m} - 0.388 + \frac{x_o}{d_m} \qquad (18)$$

where x_o/d_m is the minimum pressure location. $x_{sep,p}/d_m$ is the original predicted separation location, and x_{sep}/d_m is the improved prediction. It is seen that the accuracy can be significantly improved using this technique. While equation 18 predicts the separation locations of this data base well, its predictions for other configurations and Reynolds numbers may not be accurate.

The results of applying this technique to the prediction of pressure distributions is shown in figure 19. Inviscid theory predicts a greater expansion at the minimum pressure point and places a stagnation point at the end of the boattail. When a boundary layer calculation is added, in which the Presz cone frustum separation model is applied at the predicted separation point, the predicted pressure distribution more closely follows the experimental data. There are still significant errors near the minimum pressure point and near the reattachment point on the solid simulator. The prediction near the minimum pressure point can be improved by solving the full potential flow equations (ref. 61) as the inviscid part of an inviscid/viscid interaction program. To improve the prediction near the reattachment point will require a better model of the separated flow to be developed.

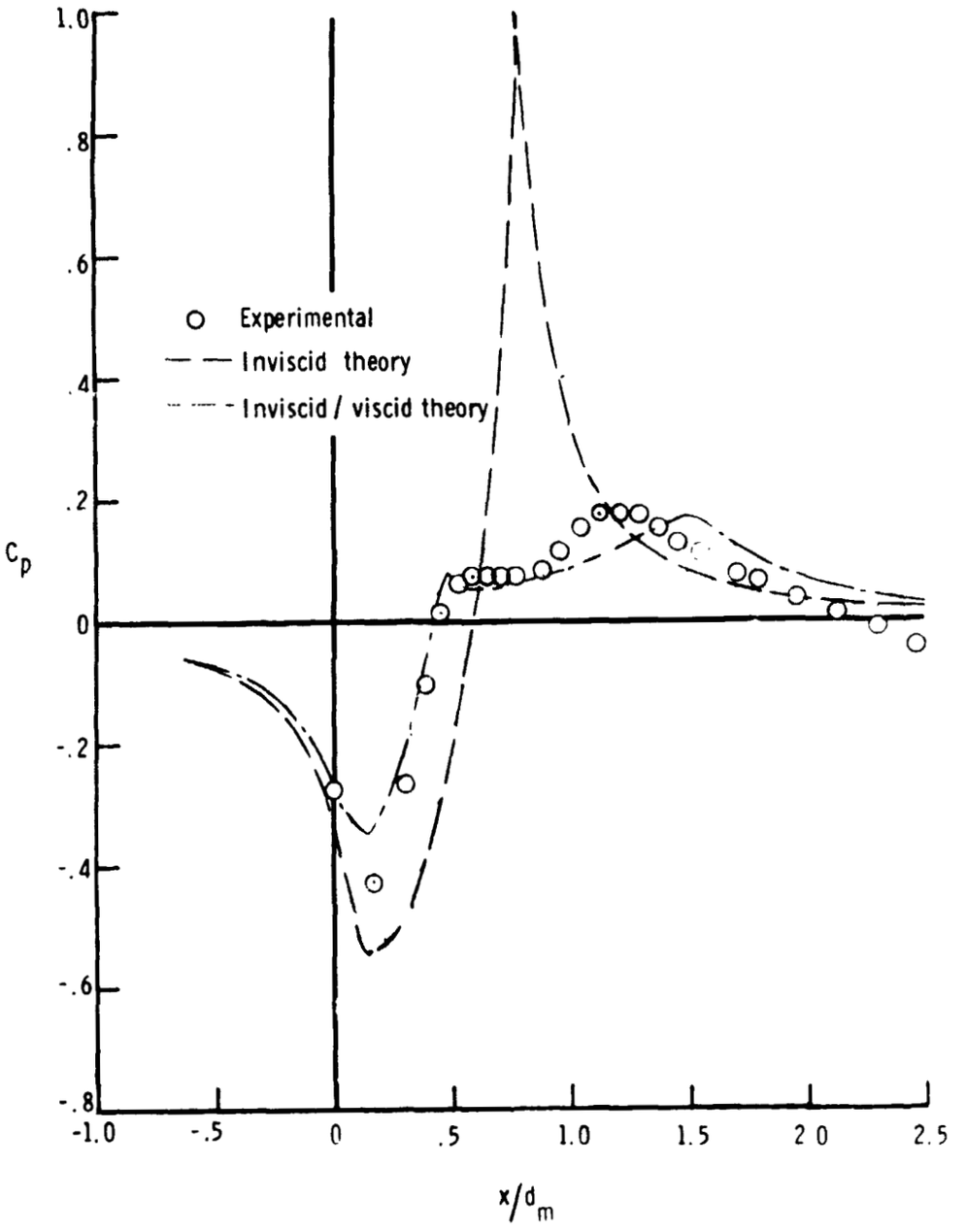

Figure 19. -Comparison of experimental and predicted pressure-coefficient distributions on a circular-arc boattail nozzle using a solid cone to represent the separated region.

(M_∞ = 0.8, l/d_m = 0.80, d_e/d_m = 0.50)

CHAPTER IV

CONCLUDING REMARKS

An investigation has been conducted in the Langley 16-foot transonic tunnel at 0° angle of attack and free-stream Mach numbers from 0.40 to 0.95 to study the phenomenon of separated flow on a series of circular-arc afterbodies. Both high-pressure air and solid circular cylinders with $d_s/d_e = 1.00$ were used to simulate jet exhausts. The results of this test indicate four primary conclusions:

1. The separation location moves forward with increasing longitudinal curvature and free-stream Mach number. At transonic speeds, shock-induced separation probably occurs, causing the separation location to move forward to the vicinity of the shock location.

2. The separation location moves little over the jet total-pressure ratio range from jet-off up to 9; however, there is a significant variance at subsonic Mach numbers with the solid simulator data because of entrainment.

3. None of the criteria tested produced accurate results in general. However, when the predictions were curve-fitted with experimental data, results were much better. Using this technique, the Reshotko-Tucker criterion gave the best results (equation 18).

4. Predicted pressure coefficient distributions are much improved when the above technique is used to predict the separation location. However, much better agreement with experimental data will be possible when an improved separated flow model is developed. This improved model should be able to handle the entrainment effects of jet exhausts. Also, a separated flow model which can vary in shape may make the pressure distribution be less sensitive to the predicted separation location.

REFERENCES

1. Reubush, David E.: Experimental Study of the Effectiveness of Cylindrical Plume Simulators for Predicting Jet-on Boattail Drag at Mach Numbers up to 1.30. NASA TN D-7795, 1974.

2. Reubush, David E.: Effects of Fineness and Closure Ratios on Boattail Drag of Circular-Arc Afterbody Models With Jet Exhaust at Mach Numbers up to 1.30. NASA TN D-7163, 1973.

3. Reubush, David E.; and Runckel, Jack F.: Effect of Fineness Ratio on the Boattail Drag of Circular-Arc Afterbodies Having Closure Ratios of 0.50 With Jet Exhaust at Mach Numbers up to 1.30. NASA TN D-7192, 1973.

4. Reubush, David E.: An Experimental Investigation of Jet Plume Simulation With Solid Circular Cylinders. NASA TM X-71963, 1974.

5. Grund, E.; Presz, W., Jr.; and Konarski, M.: Predicting Airframe/ Exhaust Nozzle Interactions at Transonic Mach Numbers. AIAA Paper No. 71-720, June 1971.

6. Harrington, Douglas E.: Jet Effects on Boattail Pressure Drag of Isolated Ejector Nozzles at Mach Numbers From 0.60 to 1.47. NASA TM X-1785, 1969.

7. Glasgow, E.R.; Divita, J.S.; Everting, P.C.; and Laughrey, J.A.: Analytical and Experimental Evaluation of Performance Prediction Methods Applicable to Exhaust Nozzles. AIAA Paper No. 71-719, 1971.

8. Wu, J.M.: Fundamental Studies of Subsonic and Transonic Flow Separation, Part I -- First Phase Summary Report. AEDC - TR-75-95, 1975.

9. Rom, J.; and Bober, L.J.: Calculation of the Pressure Distribution on Axisymmetric Boattails Including Effects of Viscous Interactions and Exhaust Jets in Subsonic Flow. NASA TM X-3109, 1974.

10. Anon.: Flow Separation. AGARD-CP-168, 1975.

11. Hess, J.L.; and Smith, A.M.O.: Calculation of Potential Flow About Arbitrary Bodies. Progress in Aeronautical Sciences, Vol. 8, D. Kuchemann, ed., Pergamon Press, Ltd., c. 1967, pp.1-138.

12. Anon.: Users Manuel for the External Drag and Internal Nozzle Performance Deck (Deck XI) - Supersonic Flow Analysis (Applicable to Deck V[illegible]). PWA-3465, Suppl. F, Pt. I (Contract No. AF33(615)-3128), Pratt and Whitney Aircraft, Sept. 1, 1968.

13. Kuhn, Gary D.: Calculation of Compressible Nonadiabatic Boundary Layers in Laminar, Transitional, and Turbulent Flow by the Method of Integral Relations. NASA CR-1797, 1971.

14. Economos, C.; and Boccio, J.: Calculation of Turbulent Boundary Layers With Heat Transfer and Pressure Gradient Utilizing a Compressibility Transformation. NASA CR-1923, 1971.

15. Hankey, W.L.: Separated Flow Studies. ARL 75-0173, 1975.

16. Calarese, Dr. Wladimiro: Review of Methods of Solution of Afterbody/ Exhaust Nozzle Flow Fields. AFFDL-TR-74-108, 1974.

17. Calarese, Dr. Wladimiro: Analysis of Transonic Viscous-Inviscid Interactions on Axisymmetric Afterbodies With Jet Effects and Boattail Injection in Separated Regions. AFFDL-TR-75-117, 1975.

18. Calarese, Dr. Wladimiro: An Analytical Method to Compute Viscous-Inviscid Transonic Flow on Axisymmetric Afterbodies Including Jet Effects and Boattail Bleed in Separated Regions. AIAA Paper No. 75-1293, Oct. 1975.

19. Cebeci, T.; and Smith, A.M.O.: A Finite-Difference Method for Calculating Compressible Laminar and Turbulent Boundary Layers. J. Basic Engineering, Sept. 1970, pp. 523-535.

20. Chow, W.L.; Bober, L.J.; and Anderson, B.H.: Numerical Calculation of Transonic Boattail Flow. NASA TN D-7984, 1975.

21. South, J.C.; and Jameson, A.: Relaxation Solutions for Inviscid Axisymmetric Transonic Flow Over Blunt or Pointed Bodies. AIAA Computational Fluid Dynamics Conference Proceedings, Palm Springs, CA, July 1973.

22. Nash, J.F.; and Hicks, J.G.: "An Integral Method Including the Effects of Upstream History on the Turbulent Shear Stress," Proceedings - Computation of Turbulent Boundary Layers - 1968 AFOSR-IFP-Stanford Conference, Vol. 1, editors S.J. Kline, et. al.

23. Coles, D.E.; and Hirst, E.A.: Proceedings - Computation of Turbulent Boundary Layers - 1968 AFOSR-IFP- Stanford Conference, Vol. 2, Stanford University, 1969.

24. Altstatt, M.C.: Evaluation of a Method for Computation of Separated, Turbulent, Compressible Boundary Layers. AEDC-TR-76-27, 1976.

25. Kuhn, G.D.; and Nielsen, J.N.: "Prediction of Turbulent Separated Boundary Layers." AIAA Paper No. 73-663, AIAA 6th Fluid and Plasma Dynamics Conference, Palm Springs, CA, July 1973.

26. Coles, D.: "The Law of the Wake in the Turbulent Boundary Layer." Journal of Fluid Mechanics, Vol. 1, Part 2, July 1956, pp. 191-226.

27. Stewartson, K.: "Corrected Incompressible and Compressible Boundary Layers." Proceedings of the Royal Society, A, Vol. 200, 1949, pp. 85-100.

28. Gerhart, P.M.; and Bober, L.J.: Comparison of Several Methods for Predicting Separation in a Compressible Turbulent Boundary Layer. NASA TMX-3102, 1974.

29. Oswatitsch, K.: The Separation Condition of Boundary Layers. NASA TT F-15, 200, 1973.

30. Sachdeva, R.C.: "A Numerical Experiment of Two-Dimensional Turbulent Separation." The Aeronautical Journal, Vol. 76, No. 740, August 1972.

31. Tsuji, Yutaka; and Morikawa, Yoshinobu: "Turbulent Boundary Layer with Pressure Gradient Alternating in Sign." Aeronautical Quarterly, Vol. 27, February 1976, pp. 15-28.

32. Nash, J.F.; and Patel, V.C.: Calculations of Unsteady Turbulent Boundary Layers With Flow Reversal. NASA CR-2546, 1975.

33. Abbott, D.E.; Walker, J.D.A.; York, R.E.: "Numerical Solution of Turbulent Boundary Layers Approaching Separation," - Proceedings of the Fourth International Conference on Numerical Methods in Fluid Dynamics, June 24-28, 1974, University of Colorado. Lecture Notes in Physics, Vol. 35, 1975.

34. Page, R.H.: "A Theory for Incipient Separation." Developments in Mechanics, Vol. 1, 1961, pp. 563-577.

35. Keith, J.S.; Ferguson, D.R.; Merkle, C.L.; Heck, P.H.; and Lahti, D.J.: Analytical Method for Predicting the Pressure Distribution About a Nacelle at Transonic Speeds. NASA CR-2217, 1973.

36. Stratford, B.S.; Beavers, G.S.: The Calculation of the Compressible Turbulent Boundary Layer in an Arbitrary Pressure Gradient- A Correlation of Certain Previous Methods. N.G.T.E.: M.330, 1959.

37. Presz, W.M., Jr.; and Pitkin, E.T.: An Analytical Model of Axisymmetric Afterbody Flow Separation. AIAA Paper No. 65, June 1975.

38. Stratford, B.S.: "The Prediction of Separation of the Turbulent Boundary Layer," Journal of Fluid Mechanics, Vol. 5, pp. 1-16, 1959.

39. Townshend, A.A.: "The Behavior of a Turbulent Boundary Layer Near Separation," Journal of Fluid Mechanics, Vol. 12, pp. 536-554, 1962.

40. Goldschmied, F.R.: "An Approach to Turbulent Incompressible Separation Under Adverse Pressure Gradients," J. Aircraft, Vol. 2, No. 2, 1965.

41. Goldschmied, F.R.: "An Approach to Turbulent Incompressible Separation and the Determination of Skin-Friction Under Adverse Pressure Gradients." AIAA Paper No. 64-465, July 1964.

42. Bradshaw, P.; and Galea, P.V.: "Step-Induced Separation of a Turbulent Boundary Layer in Compressible Flow," J. Fluid Mechanics, Vol. 27, pp. 111-130, 1967.

43. Robertson, J.M.: "Prediction of Turbulent Boundary Layer Separation," J. Aero. Science, Vol. 25, No. 8, 1957.

44. Sandborn, V.A.; and Liu, C.Y.: "On Turbulent Boundary Layer Separation," J. Fluid Mechanics, Vol. 32, pp. 293-304, 1968.

45. Sandborn, V.A.: "On the Separation of Boundary Layers," ASME Journal, 1959.

46. Gadd, G.E.: "Interaction Between Wholly Laminar or Wholly Turbulent Boundary Layers and Shock Waves Strong Enough To Cause Separation," J. Aero. Science, Vol. 20, No. 11, 1953.

47. Ross, D.; and Robertson, J.M.: "An Empirical Method for Calculation of the Growth of a Turbulent Boundary Layer," J. Aero. Science, Vol. 21, No. 5, 1954.

48. Moses, H.L.: "The Behavior of Turbulent Boundary Layers in Adverse Pressure Gradients," MIT Gas Turbine Lab. report 73, 1974.

49. Reshotko, E.; and Tucker, M.: Effect of a Discontinuity on Turbulent Boundary Layer Thickness Parameters With Application to Shock Induced Separation. NACA TN-3454, 1955.

50. Alber, E.E.; Bacon, J.W.; and Masson, B.S.: An Experimental Investigation of Turbulent Transonic Viscous-Inviscid Interactions. AIAA Paper 71-565, 1971.

51. Wu, J.M.; Moulden, T.H.; and Uchiyama, N.: Aerodynamic Performance of Missle Configurations at Transonic Speeds Including the Effects of a Jet Plume. U.S. Army Missile Command, TR-RD-76-23, 1976.

52. Hahn, Mansop; Rubbert, Paul E.; Mahal, Avtar S.: Evaluation of Separation Criteria and Their Application To Separated Flow Analysis. AFFDL-TR-72-145, 1973.

53. Ward, Vernon G.; Whitcomb, Charles F.; and Pearson, Merwin D.: Air-Flow and Power Characteristics of the Langley 16-Foot Transonic Tunnel With Slotted Test Section. NACA RM L52E01, 1952.

54. Schaefer, William T., Jr.: Characteristics of Major Active Wind Tunnels at the Langley Research Center. NASA TM X-1130, 1965.

55. Corson, Blake W., Jr.; Runckel, Jack F.; and Igoe, William B.: Calibration of the Langley 16-Foot Transonic Tunnel With Test Section Air Removal. NASA TR R-423, 1974.

56. Anon.: Flow Measurement by Means of Thin Plate Orifices, Flow Nozzles, and Venturi Tubes. Supplement on Instruments and Apparatus, pt. 5, ch. 4, Power Test Codes, ASME, 1959, pp. 5-91.

57. Braslow, Albert L.; and Knox, Eugene C.: Simplified Method for Determination of Critical Height of Distributed Roughness Particles for Boundary-Layer Transition at Mach Numbers From 0 to 5. NACA TN-4363, 1958.

58. Braslow, Albert L.; Hicks, Raymond M.; and Harris, Roy V., Jr.: Use of Grit-Type Boundary-Layer-Transition Trips on Wind-Tunnel Models. NASA TN D-3579, 1966.

59. Schlicting, Hermann: Boundary-Layer Theory, 1968.

60. Korst, H.H.: A Theory for Base Pressures in Transonic and Supersonic Flow. Journal of Applied Mechanics, Dec. 1956.

61. Wilmoth, R.G.: Analytical Study of Viscous Effects on Transonic Flow Over Boattail Nozzles, AIAA Paper 77-223, Jan. 1977.